LIGHTNING DAMAGE DETECTION ON SOLAR PANELS USING PORTABLE INFRARED CAMERA AND CONVOLUTIONAL NEURAL NETWORK FOR ENHANCING PANEL MAINTENANCE

By

ORMIILA A/P CHANDRASEGARAN

Thesis Submitted to the School of Graduate Studies, Universiti Putra Malaysia, in Fulfilment of the Requirements for the Degree of Master of Science

October 2024

FK 2024 58

Abstract of thesis presented to the Senate of Universiti Putra Malaysia in fulfilment of the requirement for the degree of Master of Science

LIGHTNING DAMAGE DETECTION ON SOLAR PANELS USING PORTABLE INFRARED CAMERA AND CONVOLUTIONAL NEURAL NETWORK FOR ENHANCING PANEL MAINTENANCE

By

ORMIILA A/P CHANDRASEGARAN

October 2024

Chairman : Faizal bin Mustapha, PhD
Faculty : Engineering

As the demand for renewable energy sources increases, the vulnerability of solar panels to lightning strikes becomes a critical concern. This research explores the correlation between lightning-induced voltage fluctuations and the resultant damage intensity on solar panels. Monocrystalline and polycrystalline solar panels were used in this study. A systematic approach was adopted, investigating the correlation between lightning-induced voltage assessment using 30kV, 60kV and 90 kV impulse voltage with multi-stage Marx impulse generator and the damage intensity on these two types of solar panels. The utility of active infrared thermography in capturing lightning-induced damage was also explored. Portable active infrared thermography equipment, tCam-Mini with wireless streaming was employed to conduct this research. Additionally, Convolutional Neural Network (CNN) based image classification techniques were integrated to enhance the efficiency of damage assessment. The application of neural networks allowed for automated and precise identification of lightning-induced damage patterns, improving accuracy and speed of image classification for damaged and undamaged samples. The experimental design involves induced lightning strikes, exposing solar panels to controlled conditions, collecting infrared images and performing neural network-based image classifications. The findings contribute valuable insights into enhancing the resilience of solar panel systems against lightning strikes, ultimately advancing the reliability and sustainability of solar energy infrastructure. A new convolutional neural network model was developed to classify the images obtained from thermography with 90.21% accuracy for grayscale and 85% accuracy on thermal images. The application of this research lies in improving the protection and maintenance strategies for solar panels, ensuring more durable and efficient renewable energy systems.

Keywords: Damage detection, Image classification, Lightning strike, Solar panel, Thermography

SDG: GOAL 7: Affordable and Clean Energy

Abstrak tesis yang dikemukakan kepada Senat Universiti Putra Malaysia sebagai memenuhi keperluan untuk ijazah Master Sains

PENGESANAN KEROSAKAN KILAT PADA PANEL SOLAR MENGGUNAKAN KAMERA INFRAMERAH MUDAH ALIH DAN RANGKAIAN SARAF KONVOLUSI UNTUK MENINGKATKAN PENYELENGGARAAN PANEL SOLAR

Oleh

ORMIILA A/P CHANDRASEGARAN

Oktober 2024

Pengerusi : Faizal bin Mustapha, PhD, PEng
Fakulti : Kejuruteraan

Memandangkan permintaan untuk sumber tenaga boleh diperbaharui meningkat, kelemahan panel solar kepada serangan kilat menjadi kebimbangan kritikal. Penyelidikan ini meneroka korelasi antara kadar voltan yang disebabkan oleh kilat dan intensiti kerosakan yang terhasil pada panel solar. Panel solar *monocrystalline* dan *polycrystalline* digunakan dalam penyelidikan ini. Pendekatan sistematik telah digunakan, terlebih dahulu menyiasat korelasi antara penilaian voltan akibat kilat menggunakan voltan impuls 30kV, 60kV dan 90 kV dengan penjana impuls Marx berperingkat dan intensiti kerosakan pada kedua-dua jenis panel solar ini. Utiliti termografi inframerah aktif dalam menangkap kerosakan akibat kilat juga diterokai. Peralatan termografi inframerah aktif mudah alih, tCam-Mini dengan penstriman atas talian telah digunakan untuk menjalankan penyelidikan ini. Selain itu, teknik klasifikasi imej berasaskan *Convolutional Neural Network (CNN)* telah disepadukan untuk meningkatkan kecekapan penilaian kerosakan. Aplikasi rangkaian saraf membenarkan pengenalpastian automatik dan tepat bagi corak kerosakan akibat kilat, meningkatkan ketepatan dan kelajuan klasifikasi imej untuk sampel yang rosak dan tidak rosak. Reka bentuk eksperimen melibatkan sambaran petir teraruh, mendedahkan panel solar kepada keadaan terkawal, mengumpul imej inframerah dan melaksanakan klasifikasi imej berasaskan rangkaian saraf. Penemuan ini menyumbang pandangan berharga untuk meningkatkan daya tahan sistem panel solar terhadap serangan petir, akhirnya memajukan kebolehpercayaan dan kemampanan infrastruktur tenaga suria. *Convolutional Neural Network (CNN)* telah dibina untuk mengklasifikasikan imej yang diperoleh daripada termografi dengan ketepatan 90.21% untuk skala kelabu dan ketepatan 85% pada imej terma. Aplikasi penyelidikan ini terletak pada menambah baik strategi perlindungan dan penyelenggaraan untuk panel solar, memastikan sistem tenaga boleh diperbaharui yang lebih tahan lama dan cekap.

Kata kunci: Kilat, Klasifikasi imej, Panel solar, Pengesanan kerosakkan, Termografi

SDG: MATLAMAT 7: Tenaga Berpatutan dan Bersih

ACKNOWLEDGEMENTS

My sincere gratitude to all those who have supported me throughout the course of this thesis.

I am deeply grateful to my supervisor, Professor Ir. Dr Faizal Mustapha, for his unwavering support and expert guidance throughout the completion of Master of Science. I would like to extend my appreciation to my supervisory committee, Dr Na'im Abdullah, Dr Murniwati Anwar and Dr Mazli Mustapha for their insightful feedback and advice which greatly improved the quality of this work. Special thanks to Dr Zuraimy Adzis for his assistance with providing resources for experimental work.

I am particularly thankful for few of my colleagues for their collaboration and discussions that made the challenging times more manageable, especially for the experimental work. I am also thankful for the lab assistants and technicians that provided guidance during my lab work.

On a personal note, I owe my deepest appreciation to my family, especially my parents, for their unwavering belief in my potential and their constant support. I would also like to thank my friends for their support and encouragement.

Lastly, I would like to thank everyone who has directly or indirectly contributed to the completion of this thesis. Your support has been deeply appreciated.

This thesis was submitted to the Senate of Universiti Putra Malaysia and has been accepted as fulfilment of the requirement for the degree of Master of Science. The members of the Supervisory Committee were as follows:

Faizal bin Mustapha, PhD
Professor Ir.
Faculty of Engineering
Universiti Putra Malaysia
(Chairman)

Mohd Na'im bin Abdullah, PhD
Senior Lecturer
Faculty of Engineering
Universiti Putra Malaysia
(Member)

Murniwati binti Anwar, PhD
Senior Lecturer
Department of Industrial Automation
Universiti Kuala Lumpur
(Member)

Mazli bin Mustapha, PhD
Senior Lecturer
Faculty of Engineering
Universiti Teknologi PETRONAS
(Member)

ZALILAH MOHD SHARIFF, PhD
Professor and Dean
School of Graduate Studies
Universiti Putra Malaysia

Date: 13 March 2025

TABLE OF CONTENTS

LIST OF TABLES

LIST OF FIGURES

LIST OF ABBREVIATIONS

°C	degree Celcius
a-Si	Amorphous Silicon
AC	Alternating Current
BIPV	Building Integrated Photovoltaics
BSF	Back Surface Field
$CaTiO_3$	Calcium Titanium Oxide
CdS	Cadmium Sulphide
CdTe	Cadmium Telluride
CIGS	Copper Indium Gallium Selenide
CIS	Copper Indium Selenide
CNN	Convolutional Neural Network
CSP	Concentrated Solar Panels
DCNN	Deep Convolutional Neural Network
DSSC	Dye-Sensitized Solar Cells
EVA	Ethylene Vinyl Acetate
GaAs	Gallium Arsenide
GW	Gigawatts
IoT	Internet Of Things
IRT	Infrared Thermography
kWp	Kilowatts Peak
m-Si	Multi-Crystalline Silicon Cells
MSE	Mean Squared Error
NDE	Non-Destructive Evaluation

OCPD	Overcurrent Protection Devices
OPV	Organic/Semi-Organic PV Panels
PET	Polyethylene Terephthalate
PID	Potential induced degradation
PSC	Perovskite Solar Cells
PV	Photovoltaic
QD	Quantum Dot
ReLU	Rectified Linear Unit
SDG	Sustainable Development Goal
SGDM	Stochastic Gradient Descent with Momentum
SIFT	Scale Invariable Feature Transform
UAV	Unmanned Aerial Vehicle
W	Watt
XRD	X-ray diffraction

CHAPTER 1

INTRODUCTION

This chapter describes the background of the research, problem statement on the damages of lightning strikes, research objectives, scope, limitations, and the layout of this research. This section briefly explains the background of types of solar panels, the types of damages that commonly occur on solar panels, and the thermography method for damage detection.

1.1 Background

Solar energy is the largest energy source on earth, and it can be used with appropriate technologies to convert it to electrical energy. As technology emerges, we seek better options to save energy and reduce our carbon footprint on Earth. Using photovoltaics would be an excellent aid for that cause. Currently, coal and natural gas are used to generate traditional electricity. These resources are scarce, but they are also harmful to the environment. This fossil fuel generation of electricity results in vast amounts of CO_2 emissions from 400 and 1000 g CO_2 eq/kWh [1]. Meanwhile, electricity generated using solar panels emitted a negligible amount of CO_2 [1]. Solar energy is a renewable energy source, so there is no apprehension regarding its depletion. Solar panels provide energy independence by enabling individuals, communities, and countries to generate electricity. This reduces dependence on imported fossil fuels and enhances energy security. Solar panels are widely used for many applications, such as residential, commercial, and industrial use. The application of solar energy spans a broad spectrum, ranging from small-scale installations to large-scale endeavours such as solar farms. The versatility of this technology is helpful for diverse geographic regions, such as urban and rural areas where electricity supply is potentially limited. This can be beneficial for communities with a lack of access to electricity for essential services like healthcare and education.

The development of sustainable goals can benefit significantly from the adaptable and sustainable nature of solar energy, which also promotes social, economic, and environmental well-being. It is essential for addressing today's issues, such as energy access and climate change, and for building a more equitable and sustainable future. We could closely relate this to Sustainable Goal Development (SDG) 7, which ensures access to affordable, reliable, sustainable, and modern energy for all [2]. Solar power systems can provide electricity in grid-connected and off-grid areas, improving energy access and reducing reliance on fossil fuels. For developing countries, this reduced cost spent on traditional electricity supply could encourage them to use renewable energy daily. Solar energy significantly reduces greenhouse gas emissions and mitigates climate change. By transitioning to solar power, countries can reduce their carbon footprint and contribute to the goals outlined in SDG 13, which seeks to take urgent action to combat climate change and its impacts [3]. Moreover, SDG 12 could be closely related to solar energy as the main aim is to ensure sustainable consumption and production patterns. Solar energy systems are resource-efficient compared to fossil fuels. As mentioned above, solar energy production generates little to no waste and emits negligible greenhouse gases or air pollutants during operation [4]. Currently, extensive research is underway to enhance existing solar panel technology, aiming to achieve greater efficiency and reduce costs, thus making it accessible to individuals across various socioeconomic backgrounds.

Since solar panel installation is a financial investment that involves small-scale to large-scale investments, such as in industries and government, the assessment of the cost and durability over their lifecycle is required. This ensures that their investment has been justified with the amount they spent over the panel's lifespan. The average lifespan of solar panels, which are commonly used, is 25 years. In these 25 years, the durability and performance must match the energy production and the cost saved on traditional electricity by using solar panels. Durability encompasses more than just longevity; it involves examining the capacity of an entity to uphold its intended function and performance amidst diverse conditions and challenges. This exploration also examines the numerous types of damage that can afflict these photovoltaic (PV) systems. From the effects of weather and environmental factors to mechanical stress, wear and tear, and even unforeseen events, we scrutinize solar panels' various challenges during their operational life.

Several types of PV panels are available in the market, such as monocrystalline, polycrystalline, thin-film solar panels and many more. The latest efficiency of monocrystalline solar panels reaches above 25% [5]. This panel has a high output of power, and it is long-lasting. Compared with polycrystalline panels, these panels are less sensitive to high temperatures. However, this panel is expensive since it is made of single crystalline silicon. Meanwhile, polycrystalline panels have lower efficiency compared to monocrystalline, around 22%, but are also cheaper than monocrystalline panels [5]. Another type of solar panel is the thin film solar panel, which is low-cost and easier to manufacture. The flexibility of these panels opens up more applications for them. Amorphous silicon solar panels are famous among thin film panels due to their triple-layered technology. However, the efficiency is up to 14% [6]. These kinds of panels are not very sensitive to temperature and can withstand climate changes, such as less sun exposure in a day [7]. Although with such advantages, crystalline panels lead the market by 90% [8]. Since solar panels provide electrical energy directly from sunlight, their efficiency has to be maintained without being interrupted by external factors. Defects are very common for solar panels as they are exposed to the outdoors. Defects such as cracking, impact damages, shading, delamination, and bubbles can be commonly seen on solar panels. This kind of surface defect leads to hot spots where the temperature of a particular area is high, and it could also damage the nearby cells [9]. Cracking can occur during installation and maintenance and also by impact by mechanical loads [9], [10]. Delamination can occur due to environmental stress, which would cause the movement of the cells [9]. This defect can occur at high and humid temperatures [9]. Shading is also common among solar panels due to nearby buildings, trees, etc. Impact damages such as falling twigs from trees or debris moved by wind cause damage to solar panels. Impact damages mostly cause cracks on the solar panels found on the surface. It can also affect the solar panel by creating a hotspot in the impacted area [11]. The efficiency of solar panels will be reduced, and the power output will be lower if this occurs.

Lightning strikes were given more importance as they are not only a natural phenomenon but a formidable challenge to the efficiency and durability of solar panels, often with financial and environmental implications. It contains high-current electric discharge and could cause serious damage when it comes in contact, including being fatal to humans [12]. The damage caused by lightning strikes on solar panels is huge because it could lead to short-circuit failure, which is permanent damage [13]. Malaysia is a country where thunderstorms and lightning are common. It is important to assess the condition of solar panels under lightning strikes because solar panels are exposed outdoors and are prone to be affected by lightning strikes. The intensity of damage from lightning strikes could vary on different types of solar panels. Detection of damages caused by lightning strikes on solar panel structures is important to determine the instances of the panels being affected. One way to detect these damages is by using thermography because solar panels could use the quick heat absorption technology to show the temperature differences on the damages.

Thermography is commonly used in non-destructive evaluation (NDE) techniques [14]. This technique is non-contact and quick to inspect damages on the surface. Normally, thermal radiation will be emitted by any object or body in a normal condition. If a body obtains external energy, it will emit infrared radiation to pay back the external energy [15]. Thermography uses this aspect and measures the temperature difference in the infrared spectrum [16]. Since solar panels use sunlight as their source, the damage to these panels is frequently examined using thermography for structural damage. However, both active [16], [17], [18], [19], [20], [21], [22], [23] and passive thermography [9], [24], [25], [26], [27], [28] have been widely used to detect damages.

Solar power is a shining beacon of innovation and sustainability in the evolving world of renewable energy. They come in various forms, each with unique attributes, efficiency levels, and applications. This research mainly focuses on detecting the damages caused by lightning strikes on monocrystalline and polycrystalline silicon solar panels using active infrared thermography. The intensity of the damage on the solar panels was studied, and the integration of a convolutional neural network for image classification was carried out as a part of the data analysis.

1.2 Problem statement

The damages undergone by solar panels are countless due to their outdoor exposure. Lightning strikes are a common phenomenon, especially in Malaysia [12]. Solar panels are vulnerable to lightning strikes due to the outdoor installation, usually installed at the top of a building or in open spaces. Previous researchers have conducted numerous tests on the damage to the electrical aspects of lightning strikes [12], [13], [29]. However, the research area of examining structural damage from direct lightning strikes on these panels is lacking. The behaviour of the structural damage could be studied to protect the structure of solar panels from creating difficulties in their operation. It will eventually lead to hot spots and could damage the nearby cells. This kind of damage can be avoided by choosing the suitable type of solar panels in a certain environment. For instance, solar panels that could resist damage or has a low vulnerability to damages could be placed in windy areas so that they would not be damaged by the slightest strike or cause micro-cracks. Highly vulnerable panels could be placed in areas with less debris.

Monocrystalline and polycrystalline silicon solar panels are different, although they are all solar panels. These panels vary in efficiency, type of material, structure thickness, etc. Despite various solar panels, the intensity of damages on these panels was never evaluated individually and compared to know their resistance towards high voltage damages such as lightning strike. According to the statistics, lightning and surge holds the highest cost of damage by percentage, 31.2%, on solar panels compared to other kind of damages [30].

The expenditure on reinstallation or repair could be reduced, thus making solar panel usage affordable for everyone. The costs of maintenance also include possible repairs, cleaning, and inspections. The presence of dirt, debris, weather-related wear and tear, and other factors have an impact on the panels' performance and efficiency. Maintenance costs are expected to decrease in coming years, but continuously being exposed to damages would cause users to spend more on maintenance, replacement and reinstallation throughout the lifetime of a panel operation [24]. The prediction cost for maintenance could be reduced to a remarkably lower cost in 2035 compared to 2010 [31]. However, the concern is that the predicted lower price is still high for residential areas and ordinary people to sustain.

Developing an efficient, portable, and cost-effective system for accurately detecting and quantifying lightning-induced damage on solar panels in real-time, leveraging infrared imaging and CNN-based algorithms to improve solar panel maintenance practices and reduce energy production losses. This problem focuses on addressing the lack of practical and precise methods for detecting lightning damage on solar panels, especially in regions like Malaysia with frequent lightning. Existing methods may be costly, less portable, or unable to provide real-time insights, which impacts the timeliness and accuracy of maintenance decisions.

1.3 Research objectives

The main objective of this research is to assess the impact of lightning strikes on solar panels using active infrared thermography, with an integrated approach that links the assessment of damage intensity variations due to different lightning strike voltages, comparison of damage intensity between monocrystalline and polycrystalline silicon solar panels, and evaluation of image classification techniques for damage detection analysis on the obtained infrared thermography images.

The specific objectives are:

1. To compare the intensity of damage from lightning strike on monocrystalline and polycrystalline silicon solar panel
2. To investigate the intensity of lightning strike damage with different impulse voltage on solar panels using active infrared thermography.
3. To evaluate the efficiency of image classification techniques, specifically using convolutional neural network, for damage detection analysis on the obtained infrared thermography images.

1.4 Scope and limitations

This study focuses on analysing structural damage in monocrystalline and polycrystalline silicon panels using active infrared thermography with a light source as the excitation method. Experimental procedures were conducted in a controlled environment to ensure consistent heating of samples, thereby preventing overheating and potential errors. MATLAB was utilized for thermal image processing and image classification.

1.5 Thesis layout

The thesis consists of five chapters. Chapter 1 includes the background of the research, a problem statement on the damages of lightning strikes, research objectives, scope, limitations, and the layout of this research. This section briefly explains the background of types of solar panels, the types of damages that commonly occur on solar panels, and the thermography method for damage detection.

Chapter 2 includes the literature review conducted for this research purpose. This chapter includes studies based on the types of solar panels available in the market, the types of damages that were detected on solar panels, infrared thermography for damage detection on solar panels and neural network integration with infrared thermal images of solar panels by previous researchers.

Chapter 3 explains the methodology for this research. The experimental work of high voltage testing to replicate lightning strikes on solar panels was presented. The properties of monocrystalline and polycrystalline panels were presented. The impulse voltage for lightning testing on samples with different intensities to evaluate the damage was presented. The environmental conditions set to standardize the test were discussed. Moreover, the setup of active thermography with parameters such as heating duration and the sample distance was presented along with the image capturing and storing process. For data analysis, this chapter presented the integration of convolutional neural network model, including model development and preparation of datasets.

Chapter 4 presents the results and discussion of the research. This section presents the research findings, including the intensity of lightning strike damage on two types of solar panels of different compositions using visual inspection and infrared thermography. This section also focuses on employing a new neural network model to address classification tasks, aiming to improve efficiency, accuracy, and reliability compared to existing pre-trained models.

Chapter 5 concludes the research findings on the damage intensity of lightning strikes on monocrystalline and polycrystalline panels and the efficiency of the newly developed neural network model on the image classification task. It also presents the contributions and recommendations for future research.

CHAPTER 2

LITERATURE REVIEW

2.1 Introduction

This section embarks on a comprehensive review through existing research and methodology related to the assessment of lightning damage on solar panels. Within this section, different types of solar panels available in the market is presented with their advantages and their popularity among consumers. Besides that, the types of damages that commonly occur on solar panels due to various factors were discussed and emphasis on lightning strike damage was presented. Relevant studies with the integration of infrared thermography with convolutional neural network (CNN) among researchers were also examined to understand the recent advancements and techniques. By synthesizing this literature, the review aims to furnish a solid framework for comprehending the current state-of-the-art methodologies, pinpointing gaps in understanding, and delineating potential avenues for future research and innovation in the field of lightning damage assessment on solar panels utilizing CNN algorithms in conjunction with portable infrared thermography cameras.

2.2 Diverse varieties of solar panels in the current market

PV cell technologies are commonly categorized into three generations. The first generation comprises conventional panels with crystalline silicon base structures, such as single and multi-crystalline silicon cells (m-Si). Amorphous silicon (a-Si), Cadmium Telluride (CdTe), Cadmium Sulphide (CdS), Copper Indium Gallium Selenide (CIGS)/Copper Indium Selenide (CIS), Gallium Arsenide (GaAs), and tandem/multi-junctions modules composed of silicon are among the materials used in the second generation of thin-film solar cells. The third generation, also called the next generation, includes cutting-edge non-silicon-based technologies and unique concepts like Dye-Sensitized solar cells (DSSC), Quantum Dot (QD) cells, Perovskite solar cells (PSC), and organic/semi-organic PV panels (OPV). These categories of panels are shown in Figure 2.1.

Crystalline silicon cells are the most common kind of solar cells [32]. Monocrystalline solar panels are made of monocrystalline silicon. This panel has a high output of power, and it is long-lasting. Monocrystalline is still expensive compared to other panels. Since it is challenging to manufacture giant crystals of pure silicon in monocrystalline solar cells, the manufacturing cost of this type of panel has historically been the greatest of all solar panel types [33]. Prices for raw silicon and monocrystalline panels have fallen over time as production methods have improved [33].

On the other hand, polycrystalline cells are more famous than monocrystalline due to their low-cost property. The processing of polycrystalline silicon-based solar cells is more cost-effective because it is made by cooling a graphite mould contained with molten silicon [33]. The cost of the panels overall has reduced since the production of polycrystalline, amorphous cells, etc. [34].

Polycrystalline panels have lower efficiency compared to monocrystalline panels [5].

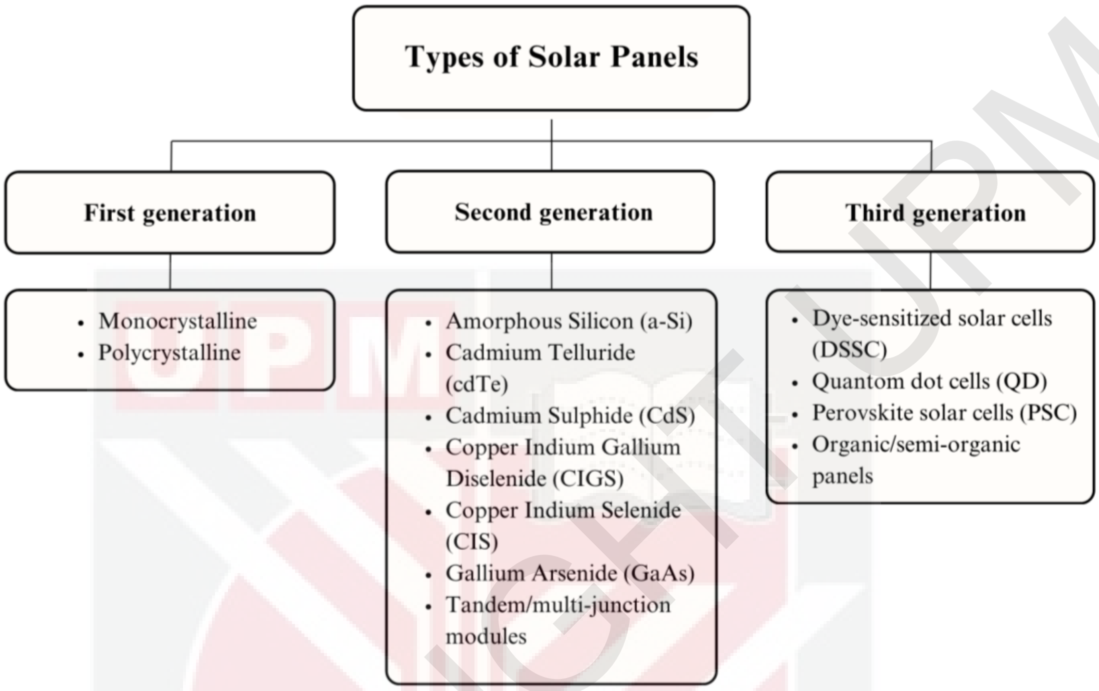

Figure 2.1: Types of solar panels available in the market

Another type of solar panel is the thin-film solar panel, which is low-cost and more accessible to manufacture. The flexibility of these panels opens more applications for them. Amorphous silicon solar panels are famous among thin film panels due to their triple-layered technology, which is cheaper than crystalline panels. These panels are not very sensitive to temperature but can withstand climate changes, such as having less sun exposure in a day but with good power output [7]. The problem with a-Si silicon is that it is less efficient per unit area (up to 14%). They are appropriate for applications where the sun only appears for a few hours because they can readily function in low-light conditions [33].

Table 2.1 presents the differences between materials, cell efficiency, temperature resistance, and lifespan between monocrystalline, polycrystalline, thin-film a-Si cells, CdTe, etc.

From Table 2.1, monocrystalline has the highest efficiency at 26.1% [5], and thin film a-Si cells have low efficiency compared to crystalline solar panels. This comparison is made because both panels are mainly silicon but have different textures. However, in terms of heat resistance, thin film a-Si cells tolerate extreme heat, and polycrystalline has less temperature resistance [12]. Meanwhile, the lowest efficiency lies with organic solar panels, ranging from 5% to 10% [15], as the material they are made of is vulnerable to the environment. Perovskite panels have higher efficiency, but their lifespan is still under research, which makes the commercialization of this panel less reliable.

Table 2.1: Classification of solar panels

Solar panels					
Variety		**Material**	**Efficiency (%)**	**Temperature resistance**	**Lifespan**
Monocrystalline		Silicon, single crystal structure	26.1 [5]	• Can withstand a wide range of temperature. • Efficiency of solar panels may decline when the temperature rises, resulting in a reduction in electricity output. • Suited to areas with warm climates.	25 to 30 years
Polycrystalline		Silicon, multiple small crystals	22.3 [5]	• Good temperature tolerance. • Excellent for a variety of climate. • Performance drop during hot temperatures is manageable.	25 to 30 years
Thin Film	Amorphous Silicon	Non-crystalline silicon	14 [6]	• Better temperature coefficient properties. • Have less of an efficiency reduction as temperatures rise. • Suited for places with a wide range of temperatures.	10-25

Table 2.1: Classification of solar panels (Continued)

	Cadmium Telluride (CdTe)	Cadmium and Tellurium semiconductor compound	22.1 [6]	• Have good temperature coefficients. • Less performance deterioration as temperature rises. • Suited for a variety of climates. • Sustain their effectiveness in high-temperature conditions.	25 to 30 years
	Copper Gallium Indium Diselenide (CIGS)	Copper, Indium, Gallium and Selenium semiconductor compound	22.6 [6]	• Moderate temperature coefficient. • The performance deterioration with rising temperatures is moderate. • Function well in a variety of temperature ranges.	5-10
Perovskite		Calcium Titanium Oxide ($CaTiO_3$)/ Perovskite	25.2 [35]	• Not suitable for raised temperature [36] • Difficulties with temperature resistance and long-term stability since some perovskite material formulations are delicate to moisture, heat, and light.	Still in research
Organic Solar Panels		Carbon based compounds (polymer/small molecules) [5]	4-5% [37], up to 9% [38]	• The stability of temperature has been an issue. • Sensitive to temperature changes. • The lifespan and efficiency of organic solar panels can be reduced by high temperatures.	Depending on materials used and environmental condition (temperature, moisture and UV light)

Table 2.1: Classification of solar panels (Continued)

Solar panel technology				
Variety	**Material**	**Efficiency (%)**	**Temperature resistance**	**Lifespan**
Building Integrated Photovoltaics (BIPV)	Various	Varies according to the types of panels used (a-Si, 6.3%; m-Si, 13.5%; CdTe, 6.90; CIS, 8.20%) [39]	• Varies according to the types of panels used	Varies according to the types of panels used
Concentrated Solar Panels (CSP)	Reflectors/mirrors	Varies according to the types of panels used	• Withstand high temperatures [40]. • The longevity of components, however, might be impacted by thermal stress and wear brought on by frequent temperature changes.	20 to 30 years
Hybrid Solar Panels	Various (eg: a-Si and crystalline Silicon, around 21%) [37]	Varies according to the types of panels used	• Varies according to the types of panels used	Varies according to the types of panels used

Several technologies have evolved around integrating different types of panels to current needs. The integration of solar photovoltaic (PV) panels into the structure of a building, such as the façade, windows, roof, and shading devices, is known as BIPV [39]. This type of technology uses various panels in their system, thus having multiple properties according to the type of panel used. Meanwhile, a big reflective surface gathers solar radiation and concentrates it onto a solar receiver with a tiny aperture area to form the CSP systems [40]. Following the conversion of the concentrated light into heat, conventional steam turbines or other heat-driven engines can produce electricity. The development of CSP technologies was confined to a few nations between the 1970s and the 1990s, with only a few research institutions and industries involved. Since 2006, the US and Spain have approved specific feed-in tariffs or power purchase agreements, significantly altering the situation [40]. With over 6 GW of projects in development and over 2 GW operational as of the end of 2012, both countries are unquestionably at the forefront of the commercialization of solar energy [40]. Australia, Italy, China, India, and others also adopted the CSP process. As a result, there has been a sharp increase in the number and diversity of engineering and construction firms, consultants, technologists, and developers dedicated to CSP [40]. Hybrid solar panels combine various solar technologies or energy-generating techniques into a single system. This may involve combining solar energy with other renewable energy sources or integrating solar thermal and PV technologies. Compared to its constituent parts, this hybrid system produces more energy per unit area than when a PV panel and a solar heat collecting panel are used separately [41].

Monocrystalline and polycrystalline silicon PV panels account for about 90% of the worldwide PV market [8]. Since crystalline silicon PVs account for a large percentage of the market, their durability and efficiency must be researched. Based on the findings, they concluded that the second generation of solar cells (thin film solar cells) had significant energy and cost efficiency advantages over regular silicon solar cells [33]. The evaluation of solar cells is based on their low prices and good conversion efficiency. Still, pure silicon and the energy-intensive process make them pricey compared to output power [33]. The type of solar panel chosen can significantly influence its lifecycle cost and market value. High-efficiency panels may have a higher upfront cost but lower lifecycle expenses due to improved performance and durability. Additionally, market demand and technological advancements play pivotal roles in determining the market value of solar panels over time.

Monocrystalline and polycrystalline has higher efficiency, while thin film technologies lacks on this aspect with efficiencies around 14 to 22 percent. High efficiency means more power generation in a smaller area which is a crucial factor for solar panels. Crystalline panels have lifespan of more than 25 years, however thin film technologies degrade faster, typically offering warranties of 10 to 25 years. Crystalline panels provide flexibility across diverse scenarios, offering more options to meet energy demands effectively. Crystalline panels produce more power per square meter, making them ideal for installations in urban areas. Since the efficiency of thin film panels are lower than crystalline panels, it requires more space to generate the same power output. Thin-film technologies have their place in specialized applications, but for most scenarios, monocrystalline and polycrystalline panels offer unmatched efficiency, durability, and long-term value.

From the works of literature, it was found that crystalline panels typically have higher efficiency rates compared to other types of solar panels. This means they can generate more electricity per square meter of area exposed to sunlight, making them more cost-effective in the long run. Both monocrystalline and polycrystalline panels are known for their durability and longevity. They are made of robust materials that can withstand harsh weather conditions and environmental factors, ensuring a long operational lifespan. Monocrystalline and polycrystalline panels have been in commercial production for decades and are widely available from numerous manufacturers worldwide. This availability contributes to their popularity and widespread use. Monocrystalline and polycrystalline panel technologies are well-established and mature, with continuous improvements in manufacturing processes and efficiencies over the years. This technological maturity instils confidence in consumers and installers alike.

2.3 Types of damages inspected on solar panels

This section reviews the types of faults or damages inspected on solar panels. The types of damage to solar panels determine the best technique to detect those damages. The faults or damages included in this section include structural and electrical damages.

Figure 2.2 shows the common factors that could affect the performance of PV panels. These factors are divided into two main categories: installation and environmental factors. These factors provide an exploration of the various elements that can impact the efficiency and effectiveness of PV panels in generating electricity from sunlight. It implies an examination of the different factors that can influence the output and overall performance of PV systems, ranging from environmental conditions like sunlight intensity and temperature to system design considerations such as panel orientation. By delving into these factors, the goal is to gain a comprehensive understanding of the dynamics that govern the performance of PV panels and how they can be optimized to enhance energy production and reliability.

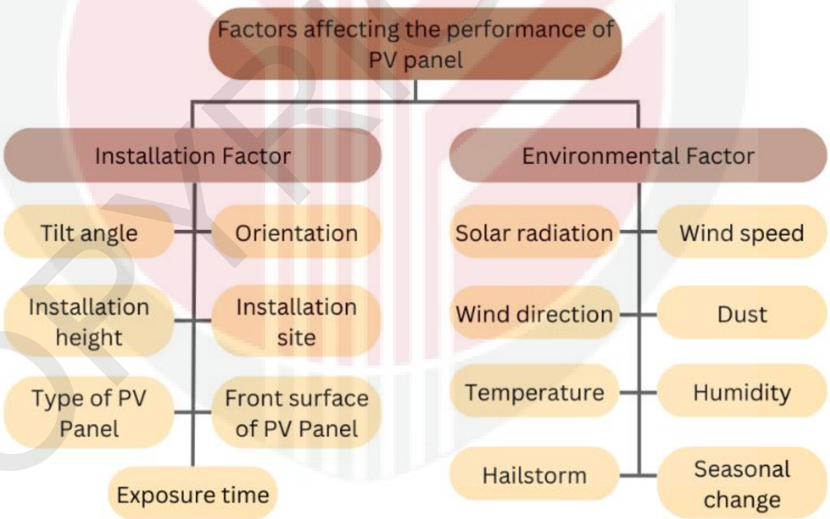

Figure 2.2: Factors affecting the performance of photovoltaic panels [42]

The performance of PV panels is influenced by various factors. Sunlight intensity plays a crucial role, as panels generate electricity from sunlight, with cloud cover, shading, and time of day affecting intensity levels. Additionally, the angle of sunlight hitting the panels impacts efficiency, with panels typically installed at angles optimized for geographical locations to maximize absorption. Temperature is another significant factor, as high temperatures

can reduce voltage output and overall efficiency, highlighting the importance of proper ventilation and cooling mechanisms. Accumulation of dust, dirt, or debris on panel surfaces can hinder performance by blocking sunlight, emphasizing the need for regular cleaning and maintenance. Shading from nearby objects, such as trees or buildings, can also significantly reduce panel efficiency. Furthermore, panel orientation and tilt, mismatch losses, inverter efficiency, degradation over time, and electrical losses within the system all contribute to overall performance. Understanding and addressing these factors are essential for optimizing PV panel performance and maximizing energy production. Based on these factors, it can be noted that panels face numerous challenges from installation to their exposure to outdoors to provide maximum efficiency.

The factors influencing the performance of PV panels are directly related to potential damages that can affect their efficiency and longevity. For instance, sunlight intensity and angle affect the amount of energy the panels can generate, but prolonged exposure to intense sunlight without proper cooling mechanisms can lead to overheating and thermal damage. Dust, dirt, and debris accumulation on panel surfaces not only block sunlight but can also trap moisture, leading to corrosion and electrical damage. Degradation is mainly caused by external factors such as dynamic temperature, mechanical stress, shock, moisture, UV radiation, etc. [43]. Understanding the relationship between these factors and potential damages is essential for implementing preventive measures, such as regular cleaning and maintenance, proper system design and installation, and monitoring for early signs of degradation or inefficiency.

Three levels of faults can be generalized: cell level, module level and array level faults [43]. These types of faults can cause damage to structural and electrical aspects. In solar panels, issues that impact specific solar cells within a PV module are called cell-level faults. These faults can manifest as reduced output, hotspots, or complete failure of individual cells within a module. Cell-level faults are typically the responsibility of the module manufacturer or can be attributed to external factors such as excessive heat or mechanical stress during operation. Individual solar modules within a PV array may experience troubles or problems known as module-level faults. These faults can result from manufacturing defects, poor quality control, or environmental stresses. Module-level faults can lead to reduced performance, safety hazards, or premature degradation of the module. Solar panel errors that impact the complete PV array instead of specific solar modules or cells are called array-level faults. Responsibility for array-level faults may vary depending on factors such as system design, installation practices, and maintenance procedures. Figure 2.3 shows examples of faults that can occur in solar panels according to the level of fault.

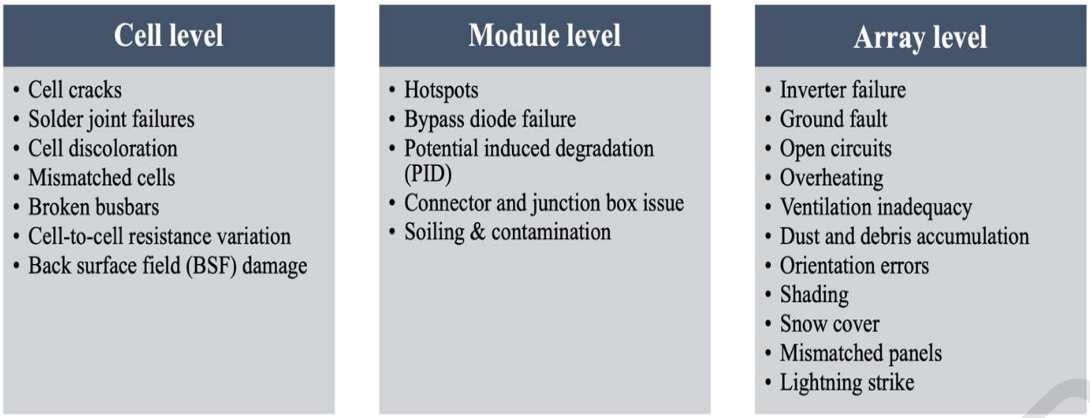

Figure 2.3: Levels of faults in solar panels and examples of faults

2.3.1 Factors affecting and causing damage to solar panels

This section presents main causes of damage to solar panels which are based on physical, electrical and environmental factors.

2.3.1.1 Physical damage

Photovoltaic panels are prone to damage during several stages of their handling, from manufacturing to installation. After the installation, the panels are exposed to the outdoors to capture sunlight, facing new challenges that could damage them. Most of these damages occur in the physical structure of the panels, such as the frames, glass surface, lamination, etc.

Failure is generally defined as an outcome that affects a system's capacity and cannot be reversed by regular operation [17]. During the manufacturing process, there are several instances where a defect could be formed on PV panels. Striation rings and moderate crystal defects, respectively, are two manufacturing defects found in monocrystalline and polycrystalline solar cells [17]. Besides that, transportation failure, clamping, cable failure, connector failure, and lightning were a few of the external causes of module failure [17]. It was noted that shocks and vibrations experienced during transit are to blame for some modules' lamination damage and glass cover breakage caused by transportation [17]. The most frequent issue that breaks glass in frameless PV modules is clamping, which happens during installation [17]. Numerous observations showed that stress on PV modules could lead to breakage. These factors include narrow clamps, sharp-edged clamp design, incorrect positioning, and overtightening of screws on module clamps during the installation process. When glass breaks, moisture can seep through the cracks and cause corrosion, compromising electrical safety and reducing performance over extended periods. However, the a-Si modules have a 10%–30% power loss in the early stages of installation due to light-induced degradation [44].

When layers within a solar panel separate from one another, it's called delamination. This usually happens when the PV cells or the materials encapsulating them detach. Adhesion contamination and environmental factors that cause humidity, moisture, and corrosion to seep into the PV module laminates are the causes of the delamination effect. The modules lose power because of optical reflection caused by the lamination failures [17]. It was revealed that variations in lamination temperatures and adhesive types could also be the leading causes of delamination [45]. Physical ageing processes associated with exposure to high temperatures may also cause a

PV module to delaminate [46]. 90% of PV modules are exposed to delamination conditions [47]. Delamination can also be observed on thin film modules and not just on crystalline panels [47]. In addition to being risky because of the possible electrical hazards associated with the panels and the installation site, the issue will be more severe if it arises near the edge of the panels [9].

Another typical damage on the panel is browning or discolouration. Ethylene Vinyl Acetate (EVA) encapsulant discolouration was first noticed at Carrizo Plains installation sites in California in the early 1990s, and it was noted to be a significant issue [48]. Besides physical damage, it is also linked to chemical damage to the panel. In extreme circumstances, the EVA discolouration indicates EVA embrittlement and concurrent corrosion brought on by dissolved oxygen [49]. However, browning usually does not cause failures; it causes the solar panel to degrade at a slower rate. Ultraviolet (UV) radiation and water at temperatures above 50°C are also among the primary causes of EVA degradation, which eventually causes discolouration like yellowing or browning [46].

Damages such as cell cracks, bubbles, snail trails, shading, and soiling cause degradation of power loss over time, and some damages pose a physical danger, such as fire failure and electric shock [47]. The causes of damages were analyzed based on the damages on PV panels. Cracking is mainly caused by installation, maintenance and mechanical loads via wind or snow [10]. Although cracking can appear during the module's lifetime, installation, maintenance, and—most frequently—transportation of the modules to their destinations is when it most frequently happens [9]. In another research, snail trails developed after defective modules were exposed to the outdoors for several months [50]. The failure can be identified with thorough microscopic imaging of the discolouration [50]. Snail trails were found to be mostly near microcracks and at the edges of cells, but it is not the cause of the defects [50]. Shading is another common problem PV modules face and could affect the performance of the PV panel. This is due to a phenomenon known as "string design," in which one "string" or shaded module in the system performs below par. Shading is most often caused by buildings, trees or any other light source, which would cause a reduction in the output power of a PV panel [9]. Solar panels were inspected at random, and faults, such as hotspots, were found that could have been caused by shading [51]. The PV system that is partially shaded harvests significantly less energy than what is predicted [52]. The findings indicate that the three-quarters shaded area experienced the most significant reductions in short circuit current, open circuit voltage, and power output, which were 66.5%, 25.3%, and 92.6%, respectively [52]. This implies that to achieve maximum efficiency and prevent shading conditions, the PV system must be installed and placed in the proper locations [52].

The formation of bubbles is another type of damage to the PV panel. This happens because gases from the released chemical reactions are trapped in the PV module. They create an air chamber with colder gas temperatures than in nearby cells [9]. The bubbles can potentially shatter the glass panel and harm the back-sealing surface, which lets humid air in [10]. Even though the

PV module's performance is not significantly decreased when this issue arises, the hot bubbles will ultimately shorten the cell's lifespan [9].

Physical damage compromises solar panels' structural integrity and can hinder their ability to efficiently convert sunlight into electricity. To prevent the risk of physical damage, it's crucial to choose appropriate mounting systems, ensure proper installation by trained professionals, and consider factors such as location and climate when designing solar panel arrays.

2.3.1.2 Electrical damage

A solar panel may experience electrical damage for several reasons, negatively impacting the system's effectiveness and performance. This type of damage can occur due to various factors related to electrical components and system operation.

Potential Induced Degradation (PID) happens when current flow may result from voltage potential between the grounded frame and the solar cells, which over time may cause degradation. PID comes in two types: reversible and nonreversible [17]. Transparent conducting oxide electro corrodes because of electrochemical reactions causes irreversible PID [17]. Current leakage occurs from the reversible PID, also referred to as surface polarization, which builds up a positive charge on a PV cell [17]. PID occurs under typical conditions at several levels, including the cell, system, module, and environmental levels. These variables are typically influenced by the cell's refractive index, type of material, system voltage, temperature, and humidity [17]. Another work used PV panels from different parts of the world, with different failures, such as potential induced degradation (PID), failed bypass-diode, hotspots, and insulation failure [22]. These damages are found using various types of inspection methods [22].

Several faults, such as partial shading, degradation of PV array, open circuit fault and series and parallel arc fault on solar panels, were found in this research [34]. However, hot spots are very commonly reported in PV modules due to short circuits [53]. It could also cause glass cracking, sintering degradation and fire risks [54]. In series and parallel montage, the PV cell with the lowest electrical performance imposes the open circuit voltage and short circuit current, respectively [55]. When a PV cell malfunctions in a short circuit, its voltage is reversed, becoming equal to and opposite to the voltage of the other cells in the series [55]. This damaged cell becomes a hot spot because it dissipates heat relatively quickly and serves as a load for other cells [55]. There is another phenomenon contrary to hotspots, which are the 'cold spots', where a cell or a group of cells in a PV system has an unusually low temperature [56]. Soldering defective cells have lower parameter variances than the other defects investigated, with local soldering faults having the most significant losses [56].

Cabling is an essential part of PV panel operation. Choosing the suitable cable is a crucial procedure that impacts the system's operation. It can also be affected by cable terminations and cable management. PV system cabling frequently involves one of three main catastrophic failure modes: arc, line-line, or ground faults. When an accidental path to ground is created in the circuit, it will lead to a ground failure mode [10]. A line-to-line failure mode is an unintentional connection made through a low-resistance path between two points in a PV panel [57]. In a grounded system, the line-line fault can be understood as a short-circuit fault; in an ungrounded system, it can be understood as a double-ground fault [58]. They are more challenging for conventional protection devices to identify and eliminate. The back-fed current into the malfunctioning string can get so tiny that the overcurrent protection devices (OCPD) are unable to clear it, according to both simulation and experimental results [58]. The fault scenarios could be caused by: "small location mismatch," "high-impedance," "low-irradiance," "night-to-day" transition fault, and the use of blocking diodes [58]. Significant contact resistance at the fault point along the fault path could result in overheating, arcing issues, or even fire hazards [58].

Arc failure mode happens when a current path in the air is created by any discontinuity in the current-carrying conductors or by insulation failure in nearby current-carrying conductors [59]. In PV systems, arc faults can be classified into two main categories: series and parallel, which include grounding arc faults [60]. Due to the significant difference in potential, parallel and grounding arc faults frequently draw high fault currents and are more straightforward to identify by conventional protection devices [60]. In contrast, the series arcing fault current—which is lower than the typical operating current level—will not be enough to melt the fuse or trigger the overcurrent protection devices because of the characteristics of PV solar cells [60]. As solar power plants age, there may be a rise in the frequency of arc faults due to high voltages, prolonged cable weathering, and ageing electronic components [61]. Prolonged arc faults can potentially ignite the surrounding area and the insulation. If the sunlit modules still power the cabling, this could be hazardous for firefighters and residents in the case of rooftop systems [61]. Typically, incorrect cable selection or mismatched connections between PV modules and related components have been linked to connector failures. These malfunctions can occasionally result in the string losing all power, which can cause electric arcs and fires [17]. Inadequately designed or concealed junction boxes allow moisture to enter, corroding the connections inside. This results in internal arcing due to wiring failure [62].

A voltage mismatch happens when there is uneven hard dust on several strings that are connected in parallel [63]. Different parallel strings attached to a standard inverter provide varying voltages to the inverter in this condition, known as partial shading [63]. Because of this, the inverter finds it challenging to find the ideal voltage point at which to deliver the most power [63].
Meanwhile, another study presented eight types of faulty panels for inspection, which are primarily scheduled for maintenance. The panels were categorized according to the severity of the fault to avoid power outages [83]. This fault analysis system could also suggest maintenance measures for the faults the PV modules face [64].

To reduce the risk of electrical damage, it's essential to employ proper grounding and surge protection measures, ensure the use of high-quality electrical components, and adhere to safety standards and regulations during installation and maintenance.

Table 2.2: Comparison of electrical faults on solar panel reliability and safety

Aspect	Hotspots	Arc faults	Series/parallel fault
Primary cause	Shading, soiling, cell defects, short circuit	Loose connections, damaged cables, high voltage, ageing electronic components	Open or short circuits in wiring or cells
Impact on efficiency	Reduces affected cells/panel performance, glass cracking, sintering degradation and fire risks	May lead to system shutdown	Decreases output in affected strings/modules
Safety risk	Overheating can cause fire	High fire risk	Can lead to overheating

2.3.1.2 Environmental damage

Several studies have compared the types of damage and their performances over the years in different countries where they were exposed to unique environments. Natural phenomena could damage solar panels because they are exposed to the outdoors and are prone to damage.

Heavy hailstorms on PV panels were investigated for their performance, and their behaviour was simulated [65]. These modules were placed in 3 different places around the south of Austria [65]. Hailstones up to 40mm were dropped on these modules, and visible damage was observed on the glass panels, such as cracks, breakage and fractioned cells [65]. Hailstorms can cause cracks [66]. Heavy hailstorms may cause damage to the glass surface and solar cell fracture [67]. When cracks occur in a solar cell, the components that are split from the cell are unlikely to be completely detached; however, the series resistance across the crack is determined by the distance between the cell parts and the number of cycles for which the module is twisted [42]. The severe consequences of cell cracking on PV module output power are not visible right away but rather over time when the modules are stressed by thermal cycling, humidity, and physical loading in the environment. As a result of the power loss caused by these cracks, cells may become electrically disconnected or dormant [42]. Hailstorms shorten the life of PV modules and lower overall power generation [42]. The characteristics of a hailstorm, such as the quantity and size of hailstones that fall in a given area and the wind speed during a hailstorm, determine the damages that result [42].

In colder regions, snowfall poses serious risks to PV technology. The snow and ice accumulation on the panel surface blocks sunlight from entering the solar cells, lowering the energy produced. With a shallow snow layer on the solar cell's surface, PV performance was down 13% on a clear day, and on a cloudy day, it was down 40%, according to research conducted in Russia [68]. However, a thin layer of snow covering the solar cell does not cause a significant reduction in its performance [68]. In research conducted in Colorado and Wisconsin, snow-related monthly PV system energy losses were measured to reach 90% [69]. The percentage of annual energy production that was lost varied from 1% to 12% [69]. Another research conducted in Michigan, USA, stated that yearly energy losses ranged from 29% to 34% because of snowfall [70]. It was observed that the tilt angle and the level of ground interference significantly impact the energy losses caused by snowfall [70].

Another common condition is dust storms or dust accumulation on PV panels. In some regions, dust is also called sand or sand storms. Many studies have examined the impact of dust accumulation on PV system performance. The findings showed that the site's weather significantly influences how quickly dust accumulates. A dust storm can cause an output power reduction of 20%; if modules are not cleaned for longer than six months, a decrease of 50% may occur [71]. An experimental study on a decline in PV output efficiency revealed that when the dust deposition density was roughly 8 g/m^2, the efficiency reduction could reach 11.6% [72]. PV output power decreased by 6%, and after 45 days of exposure, glass cover transmittance decreased by 20% after five weeks of exposure, and 5 g/m^2 of dust was left on the PV glass surface, which was experimented in Dhahran, Saudi Arabia [73]. The average rate of efficiency degradation for monocrystalline PV panels, which were tested in Baghdad, Iraq, for dust accumulation, is 18.74% (1 month), 11.8% (1 week), and 6.24% (1 day) [74]. Dust deposition also resulted in a temperature variation between the cleaned and dust-deposited panels, which in turn caused a slight fluctuation in the short-circuit current and a significant drop in the open circuit voltage [75]. Winter months' soiling rates were higher than summer soiling rates. It is believed that condensation that formed on the modules early in the morning caused dust to stick [76]. A solar test facility at

Qatar Foundation, Doha, showed that January through February saw the highest soiling rates, while June through July saw comparatively flat soiling rates [76].

An outdoor experimental study in Sohar, Oman, was conducted to investigate the impact of dust and cleaning on the performance of PV modules [77]. Four PV modules, two monocrystalline and two polycrystalline, each with a 100 W rating, were installed and tested horizontally for an entire year. Microscopic and X-ray diffraction (XRD) analyses were performed to determine the size and composition of the dust particles accumulated on the modules. The degradation differed for different PV technologies, with monocrystalline modules showing more reduction than polycrystalline modules. After 55 days of dust accumulation, the power degradation of monocrystalline modules was 40%. The highest power degradation was observed in August. The efficiency of the monocrystalline PV module ranged from 9.24% to 10.76%, while the PV performance ranged from 52.76% to 72.81%. Despite the dust accumulation, the monocrystalline PV module showed promising behaviour and characteristics in Oman [77]. Dust accumulation lowers the panels' efficiency by 11.86% and power output by 8.80%, whereby the paper suggested regular cleaning following the weather conditions [52]. Partial shading and power loss were observed in research conducted under climatic conditions in Algeria, which is prone to sandstorms [78]. The effects of sand accumulation and partial shading were examined on PV panels in a desert setting for two months in Adrar [79]. According to the study, partial shading caused an output drop from 79.7 W to 16.45 W [79]. The panels' prolonged exposure to the desert environment weakened the modules, causing delamination and encapsulant discolouration.

A study on installations outdoors in India found that thin film and silicon PV modules degrade at 1.5% and 0.7% per year, respectively [80]. In the desert, the drop in power production of crystalline Silicon PV modules was estimated to be roughly 1.1 every year [81]. Due to the increased stress induced by the high number of expansion-contraction cycles, modules with less operation can deteriorate quickly [82]. PV modules are significantly damaged by numerous failures such as EVA browning, cell connection ribbons browning, and solder bond corrosion, according to the results of a visual and thermography examination which was exposed under climatic conditions in sub-Saharan Ghana [83]. The study evaluates the long-term dependability and performance of monocrystalline PV modules in an off-grid PV system subjected to tropical climatic conditions in Ghana's sub-Saharan region after twelve years of operation [83]. With an average loss of 3.19% annually, their power output has decreased by 34.6% from 41.4% [83].

Besides that, impact damages such as falling twigs from trees or debris moved by wind cause damage to solar panels. The effect of this damage would also cause power reduction in the output. Impact damages mainly cause cracks on the solar panels, which are found on the surface. It can also affect the solar panel by creating a hotspot in the impacted area [11]. It was also discovered that the PV module covered in bird droppings reduced the PV system's output power by roughly 7.4% [52]. Another study demonstrates that bird droppings significantly impact solar PV cell performance; based on rainfall and tilt angle, they can reduce output power by as much as 23.8% in March (at 0° tilt angle/horizontal) [84]. Output can be significantly decreased by shading on a small number of cells (in the case of bird droppings) across several strings where the experiment was conducted on shading randomly on cells [85].

To mitigate environmental damage, durable materials, proper sealing and insulation techniques, and consideration of factors such as location and climate must be used when designing and installing solar panel systems.

2.3.2 Lightning strike damage and impacts on solar panels

Environmental damage to solar panels, such as exposure to extreme weather conditions, can weaken their structural integrity and increase susceptibility to lightning strikes. Lightning strikes are common and a natural phenomenon that could not be avoided. It contains high-current electric discharge and could cause severe damage when it comes in contact, including being fatal to humans [12]. The damage caused by a lightning strike on solar panels is massive because it could lead to short-circuit failure, which is permanent damage [13]. When lightning strikes a solar panel array or nearby structures, it can induce high voltages and currents in the system, leading to catastrophic failure and safety hazards. Direct lightning strikes on solar panels can result in physical damage, such as shattered glass, melted components, or structural deformation. Additionally, the intense heat generated during a lightning strike can cause localized overheating and thermal damage to panel materials.

In overall damages on solar panels, lightning strikes and surges hold 26% of the damage for these panels [12], and a statistic from 2005 to 2014, which is represented in Table 2.2, shows lightning surge holds 31.2%, which is the highest among the causes of damages to solar panels [30]. Damages caused by lightning strikes include defects in bypass diodes, broken glass and arcing at string ribbons on solar panels [12]. Several damages occur on the inverter, cables, solar tracker and security systems [12].

Table 2.3: Statistics data for causes of damage to Solar PV systems by damage costs (2005-2014)[30]

Types of damages	Costs of damages by percentage
Maloperation	0.8
Vandalism	0.5
Theft	1.8
Water, flooding	1.4
Fire	23
Structural/material defect	10.9
Storm, snow load, elementary	18.3
Animal bite	8.6
Lightning and surge	31.2
Other damages	3.3

Two scenarios of the assumption of direct lightning strikes were presented in their paper [86]. In the first example, the panel is destroyed [86]. The panels underwent exposure to fire, exhibiting damage reminiscent of that caused by lightning strikes. The panel frame and semiconductor structures were melted. The second scenario is far more prevalent and difficult to recognize [86]. Overvoltage causes panel damage, and the semiconductor structures are severely faulty, although the panel appears unaffected or the deterioration is barely visible [86].

Another study investigated the unwanted signal coupled to a solar panel due to the induced voltage. It found that as the distance between the solar panel and spark discharge increases, the damage to electrical equipment becomes more serious [29]. Another research tested their sample with heat treatment until the appearance of a bubble at its insulation layer and with lightning impulse voltage [87], [88], [89]. The samples that were not heat-treated withstood thousands of lightning impulse voltage tests until they failed. The maximum power output fell under 80% of their actual values, and the samples showed no evidence of damage during visual inspection [87]. When the same conditions were applied to a sample with heat treatment-generated bubbles, the module was damaged after only 12 shots of lightning impulse voltages [87]. The impact of lightning impulse voltage applied to polycrystalline silicon PV modules with comparatively low peak voltages (15 V, 30 V, and 90 V) was investigated in this article [88]. According to the findings, the repeated lightning impulse voltage stress causes the modules to deteriorate even at lesser magnitudes [88]. It shows that the electrical deterioration of the module caused by the lightning impulse voltage leads to the PV module's breakdown. Another research conducted a direct lightning strike on a PV panel and found that the lightning strike against a PV panel can be prevented if the frame is grounded so that the surface discharge occurs [90].

Despite many factors contributing to lightning damage, it was found that variations in cable length did not affect the lightning-induced overvoltage when the samples were exposed to direct lightning strikes [30]. Meanwhile, the endurance of PV module insulating encapsulation against voltage was evaluated with two experiments [91]. A lightning impulse voltage test was carried out on solar panels. Ringing oscillations were found in the PV modules, which had undergone degradation caused by partial discharge [91].

Direct lightning discharge primarily affects the structural integrity of the PV panel and can cause fires in the electrical distribution system and nearby installations [92]. The electrical properties of PV systems are examined under direct and indirect lightning exposure in this research, and it was found that under the impact of a lightning discharge, the overvoltage created in the PV test bench is around 10-15% of the value of the lightning surge [92]. The lightning performance of a 100kWp PV plant is investigated using various string geometric designs [93]. It is found that critical parameters that greatly influence the range of generated surges include lightning characteristics (peak current, front time), lightning hit position, created loop surface, and soil resistivity [93].

When lightning hits, it indicates that a transient current emerges at the nearest point to the strike, and the value of the transient current matches the lightning current [94]. A high voltage transient arises on the AC side of the inverter in a solar PV system, causing significant harm to the inverter [94]. Based on these findings from [13], lightning strikes might cause damage to the solar PV array and inverter, resulting in a high replacement cost. Even though lightning was injected between the solar PV modules and the inverter, the transient voltage and current could travel along the conductor and harm other components, especially the solar PV modules and inverters [13].

The risk of human life loss or injury, the chance of PV damage causing service interruption, and the chance of economic loss are all factors that must be considered when estimating the hazard of lightning strikes [95]. In the case of a lightning strike, however, the electrical utilities of the structure may be put in jeopardy [95]. Various types of damage have been studied in past research, especially electrical damage to solar panels. The types of electrical damage caused by lightning strikes is presented in Table 2.3.

Table 2.4: Electrical damages caused by lightning strikes [30]

Components	**Type of damage**
Solar module/array	Defects on electronic parts, cracking on the surface, fire hazard in the electrical distribution system and nearby installations [92]
Inverter	Defects on electronic components [13], data communication parts, fuse or circuit breaker tripping [94]
Combiner box	Burning and melting due to short circuit event, breakdown of sensitive components inside the combiner box, induce voltage surge [88]
Cabling	Burning and holes in insulation of cables, arcs of electricity, electromagnetic interference, overvoltage

Lightning strikes can cause structural and electrical damage to panels, decreasing efficiency and potential system downtime. Researching lightning threats on PV systems has become a hot topic in recent years as PV has grown in popularity as a sustainable energy source. Structural damage from a lightning strike, if left unchecked, can worsen over time due to exposure to environmental elements such as rain, wind, and sunlight. Identifying and addressing the damage early helps prevent further deterioration, prolonging the lifespan of the solar panel. Therefore, addressing environmental vulnerabilities and implementing lightning protection measures are essential to mitigate the risks associated with environmental damage and lightning strikes on solar panels.

2.4 Infrared thermography in damage assessment for solar panels

This section reviewed literature based on infrared thermography on solar panel damage detection. Thermography is commonly used in non-destructive evaluation (NDE) techniques [14]. This technique is non-contact and quick to inspect damages on the surface. Normally, thermal radiation will be emitted by any object or body in a normal condition. If a body obtains external energy, it will emit infrared radiation to pay back the external energy [15]. Thermography uses this aspect and measures the temperature difference in the infrared spectrum [16]. Since solar panels use sunlight as their source, the damage to these panels is frequently examined using the thermography method for structural damage. However, both active [16], [17], [18], [19], [20], [21], [22], [23] and passive thermography [9], [24], [25], [26], [27], [28] have been widely used to detect damages. Previous research shows that both methods were used to detect solar panel damage according to the application and environment.

2.4.1 Passive thermography

Passive thermography does not require a heating or excitation source. It is commonly used for large-scale solar plants. This technique uses solar energy to heat up solar panels, which convert heat energy to electrical energy. The heated panels can be tested using a thermal camera for damage, especially for hot spots.

The use of passive thermography combined with GPS and CNN, was presented in [24]. This method claimed to detect the faults automatically with pattern recognition with the aid of artificial intelligence [24]. The passive thermography method was reliable in detecting hotspots or damages in the circuit because of the temperature difference [26]. The dirt on protection glass was also studied using passive thermography [27]. The temperature distribution found in this study was unusual, with variations of about 6°C caused by dirt [27].

Infrared thermography is significant in detecting damages or defects on the surface and within the material, such as failures within building walls, thus making it easier and faster to detect defects within solar panels [9]. Using thermography shows the overheated surface of PV panels due to shading [9]. It is stated that thermography is time-saving and also an inexpensive method to identify most issues related to surface defects, external and internal cell problems [9].

Seven faulty modules were used in this research to detect damage on rooftops using passive thermography [90]. The obtained thermal images were divided into sub-windows to make them easier to analyze. This technique claimed to aid with remote monitoring and save time for detection with high classification efficiency [28].

Excessive reverse bias occurs when shading occurs, and the cells overheat, eventually damaging themselves [92]. This will eventually cause power loss. Some defects, such as ageing problems or degradation, can be detected with visual inspection [92]. However, thermography is recommended to detect defects such as deposition, shading, or bubbles at the back of the panels [96]. It was proven that hot spots are not visible with the naked eye but visible with thermography [96]. IR thermography was used to assess a few samples with damage on PV panels along with the application of IoT [34]. The accumulated dust part on the PV panel showed a lower temperature compared to the surrounding cells [34].

Indoor thermography in a dark environment was carried out using a voltage supply [93]. For outdoor illuminated thermography, the images were taken at 1000 W/m^2 [93]. However, for a normal case, 600 W/m^2 is sufficient. Temperature modulation was performed to show better results by modulating current flow conditions [97]. However, normal outdoor thermography images show fewer defects than indoor images [97]. Meanwhile, the improved outdoor method produces clear information about defects [97].

Aerial thermography has become popular in recent years. Large solar installations could benefit from this technology using passive thermography to inspect for damages. Drone images were considered helpful with current technology for visually inspecting solar panels and GPS information to locate the damages [98]. Aerial thermography has advantages such as detecting damages without planning beforehand and inspecting PV power plants without interrupting operations. Aerial thermography with a remote-controlled helicopter was used by installing a thermal camera on it [94]. This technique has a few advantages, such as the fact that this system is faster, automated, and low-cost compared to person-hour involvement, has low health hazards, and can inspect accurate and inaccessible areas [98]. Similarly, a thermal camera beneath a quadcopter was installed to carry out passive thermography [32]. Another research presents a unique method for detecting solar panel defects using data from a condition monitoring system mounted on an unmanned aerial vehicle with GPS [99]. This system can evaluate huge solar plants with thousands of solar panels, saving thermographic inspection time and costs [99].

Another remarkable work included in this research is that they used UAVs with thermography to detect the faults in PV modules [24]. By the end of this research, several hot spots were detected using thermography [24]. However, another common issue was discovered during the aerial inspections: hot spots caused by soiling and vegetation shadowing PV cells are hidden from the camera vision [100]. They are not considered defects but can impact the aerial IRT results and total PV plant downtime [100].

Another research aims to detect dust in PV panels using unmanned aerial vehicle [97]. In all instances, the findings are verified using a thermographic camera because the objective of the study is to use a radiometer sensor with a condition monitoring system on an unmanned aerial vehicle [101].

Despite having numerous advantages, this method has some limitations based on past literatures. The thermography images collected had a ‘Heat Island Effect’ due to the reflections, where the land and the panels' temperatures were almost similar [51]. In another thermography video sequences collected, they had trouble with motion blur, video freezing, sun reflection, shadowing, etc. [102]. Reflection was stated to be a common problem in thermography [24].

2.4.2 Active thermography

Active thermography requires a heating or excitation source to generate the heat flow. This heat flow will show the temperature difference between damaged and undamaged structures. Active thermography is divided into four techniques: pulsed, long-pulse, lock-in and vibrothermography [103]. Among them, pulsed thermography is commonly used because it is quicker [103]. For long-pulse thermography, the heat is supplied continuously with a low-power heating source [103]. Vibrothermography differs slightly from the others because it converts mechanical energy into heat energy, generating hot spots in damaged areas such as cracks [103].

This paper presented faults such as broken cells, short circuits, open-circuited modules, etc., which were detected using the thermography method with a thermal camera to assess the damages [17]. Furthermore, the proposed method in this paper stated that it can improve efficiency, productivity, and safety in a situation [17]. Moreover, it has the advantage of covering a large space of PV modules [17].

Thermography can detect faults such as damaged cells, hot spots and fire hazards in PV modules [16]. The heating duration for excitation source ranged from 3 to 10 seconds by heat radiation transfer, and the cooling process was recorded [18]. The heat that passes through a defect will accumulate the heat, thus increasing the temperature [18]. Another research applied lock-in thermography to study the power loss in PV cells [19]. A step heating thermography using different excitation lamps, such as halogen lamps and LED lamps, was carried out [20]. It was found that halogen lamps are good excitation source for thermography [16].

Meanwhile, another research used eddy current thermography, which is another form of active thermography with lock-in and pulsed thermography [21]. This research used an induction heater as an excitation source [21]. Since the penetration depth of thermal waves are good, this research claimed that they could detect micro defects on the surface [21]. For pulse eddy current, the generator excites the electromagnetic induction with the pulse generated, thus producing high-frequency AC [21]. Dark and illuminated lock-in thermography using pulsed current as the excitation source could detect small temperature differences within the surface [22]. Regarding cost and time, this method was considered efficient and reasonable, with promising results [22].

Electrothermography was used to detect defects in silicon PV panels, and it was found to be effective in detecting external defects compared to the electroluminescence method [23]. Meanwhile, this study's particular power inverter with bidirectional power flow was considered time-saving [104]. The current was injected into the samples. They carried out active thermography in both illuminated and dark conditions, indoors and outdoors, where the defects showed cold spots [104].

A comparison of the electroluminescence method, photoluminescence imaging, and infrared thermography was presented [78]. External current was used as a heating source during dark conditions [78]. It's feasible to assess the thermal behaviour of cells in a module and spot various flaws, such as short circuits, shunts, and inactive cells [14]. However, it was found that not all detected flaws result in a temperature rise [14].

Thermography has several advantages, such as that it is a non-destructive testing technique and that no contact with the sample is required [16]. Moreover, it is a portable system, and it is safe for users as well [16], [103]. Since this method has no direct contact with the surface, it is not hazardous for humans and the material's property [103]. Moreover, in the case of solar panels, which are sensitive to temperature, this method has shown significant accuracy in defect detection (up to 99%) [103]. Thermography in PV modules is very helpful because it can detect faults or damages that electrical measurements cannot detect [16].

The drawback of this method is that larger surface areas are hard to detect with this technique, as active thermography requires an excitation source [16]. It is stated that the images from infrared cameras are noisy when the camera resolution is low [21]. The equipment cost is higher, and image resolution could be easily disrupted by the environment and the camera quality, where we would need image processing to improve it. Longer measuring time such as for long-pulse technique is a drawback for this method [22]. From these methods presented, thermography could detect all of them except for isolation failure, snail tracks and yellowing because there is no temperature difference from these defects [22]. One of the challenges in thermography is the reflection problem. Emissivity is also another factor that causes errors in thermography. A standard test is recommended when conducting active thermography [43].

Despite having drawbacks, this method is found to be a very useful way to detect damages on solar panels because of its accuracy. Since the equipment is also portable, it is easier to carry out this method at different places. Active thermography is popular because of the reliability of the technique. The excitation source could aid with heating up the solar panels to detect damages unlike passive thermography where the heating source is sunlight, and it can only be carried out during sunny days. Meanwhile, active thermography can be carried out at night and also when the weather conditions are poor, which makes it more reliable. With active thermography, the excitation source can be carefully controlled and applied selectively to target specific region of interest. This can reveal defects or damage that might not be detectable under normal conditions. By actively inducing thermal contrast, active thermography can often achieve higher sensitivity in detecting subtle changes or anomalies in the material. Active thermography techniques often involve capturing thermal images in real-time while the material is subjected to the excitation source. This dynamic imaging allows for the observation of transient thermal responses that can provide valuable insights into the nature and extent of the damage. In contrast, passive thermography typically relies on thermal radiation emitted by the material itself, which may not always provide sufficient contrast for detecting subtle defects.

2.5 Neural network application in image classification for infrared images

This section delves into the research and development of using neural network architecture to classify infrared and thermal images. This section comprehensively explores existing studies, methodologies, and advancements in the field, understanding the integration between neural networks in image classification of infrared images of PV panels.

Pre-processing and data augmentation is an important process when training neural network model. Pre-processing help remove irrelevant information or noise from the data, improving the quality of input data for the neural network. This makes it easier for the model to learn relevant patterns when training. Moreover, it will also aid with effective feature extraction process. Cropping out the region of interest is one of the method used by researchers [105], [106], [107], [108]. Individual solar modules were cropped out of the thermal images and any potential false hotspots were removed from the datasets [106].

Effectively removing non-decision relevant information from the images, such as background elements, and visually highlighting the object area enhanced the model's prediction performance [105]. Grayscaling, thresholding and applying filters such as box-blur and Sobel-Feldmen filter was applied as a pre-processing method for the dataset [109]. Contrast enhancement were also used by several researchers to improve the images to extract the features from the datasets [110], [111].

By presenting the model with a wider variety of examples, data augmentation helps prevent overfitting. There are several techniques employed by researchers for this process. One of the most common way of data augmentation is flipping and rotating the images. Flipping of images was carried out in infrared images in these research [106], [111], [107], [108], [112]. Image rotations with 90°, 180°, and 270° [106], [110] and ±45° [105] were carried out to randomize the data. Another research implied rotation of images by ±90° to reduce differences between landscape and portrait orientation of modules [111]. Scaling and shifting is also another way of data augmenting the images. Scaling and shifting (0–20°) with noise [113] and rescaling by ±25% [105] were carried out for better feature extraction. Data augmentation helps the model become more robust to changes in the input data that it might encounter during deployment. This will also reduce biases in training dataset and allows practitioners to train effective models even when the dataset size is limited.

There are several ways of utilizing neural network model to achieve the goal of classification such as developing new network models from scratch and transfer learning method or combination of both methods. Transfer learning is a method of knowledge being transferred between several models and the acquisition of new tasks considers previously learned information [114]. Aerial infrared images of PV modules used with ResNet-50 can diagnose the top 10 common defects in modules with testing accuracy above 90% by using transfer learning method by replacing the original fully connected layer with randomly initialized fully connected layer of 11 neurons [111]. Using a scale-invariant feature transform feature descriptor, spatial pyramid matching, and deep learning techniques, infrared pictures were used to categorize PV panels into defective and non-defective with 91.2% accuracy and defects (block, patchwork, single, and string) identification with 89.5% accuracy [106]. The findings indicate that the VGG-16 and MobileNet models outperform the random forest classifier and scale invariable feature transform (SIFT) descriptor combination using transfer learning method [106]. The final fully connected layers in those pre-trained models were replaced with four-neurons [106]. Using the transfer learning technique, ResNet-50 was trained to classify infrared photos of objects hidden underneath their clothes and improved their model's performance by fine-tuning a total of 900 images in their fully connected layer [105]. Another research used a combination of small DCNN model and transfer learned VGG-16 for the classification of faults [115]. The findings shows that VGG16 performs better than DCNN model with accuracy up to 99.8% [115]. Similarly, an Enhanced CNN model with transfer learned GoogleNet were used and the findings concluded that the transfer learning method can diagnose defects effectively compared to the enhanced model [108].

A combination of a ResNet-34 and a U-Net was used to carry out semantic segmentation [116]. One drawback of semantic segmentation is its inability to distinguish between distinct PV modules [116]. However, the YOLO object detector is unaffected by this issue. Nevertheless, it is limited by the inaccurate way PV modules are represented, as bounding boxes are used instead of segmentation masks [117].

An isolated deep convolution-based neural model with a quick, low-storage architecture was developed to categorize PV panels into three health-based categories with 96% accuracy [113]. Using a fresh dataset of infrared images that had not been utilized for training or validation, a transfer learning technique was applied to the same isolated created model in eight minutes to identify the problems in the PV panels that had been initially placed in a hotspot and were faulty with 97.62% testing accuracy [113]. Similarly, transfer learning is applied using a pre-trained base model from a collection of PV cell electroluminescence images and then fine-tuned to infrared images [107]. The findings demonstrate that the transfer learning technique can enhance performance to an average accuracy of 99.23% [107]. Isolated model with the combination of transfer learning method has shown promising results with 99.23% accuracy [107].

The accuracy of the proposed CNN model in fault classification is 97.42%, compared to 93.04%, 91.25%, 83.70%, and 94.30% for AlexNet, VGG16, ResNet18, and Akram's models, respectively [110]. Richer and more thorough feature information was extracted using varying filter bank levels, and the integrity of feature information is effectively preserved with Res-Model [110]. A light CNN architecture is used to train an isolated learned model from scratch, achieving an average accuracy of 98.67% [107]. Similarly, isolated convolution neural networks were proposed to classify infrared images based on dust and hotspots 98% accurately [109]. IR thermographs of eight distinct panels, seven defective and one healthy, were employed to extract textural information. Then, using a scaled conjugate gradient back propagation algorithm, the weight of the neural network classifier was adjusted, resulting in a testing accuracy of 91.7% [28]. When it came to detection, 92% of undamaged PV modules and 93% of damaged modules could be accurately identified by the developed CNN model based on their infrared image pattern [118]. This supports the use of CNNs to provide autonomous problem detection in solar power facilities, thereby reducing the need for system interruption and streamlining operations and maintenance [118]. A deep CNN classifier shows great efficiency for binary and multiclass classification with 98.71% accuracy and this approach has proven to be better than machine learning based algorithms [112].

Performance metrics are used to assess the performance of models in classification. Common performance metrics include accuracy, precision, recall, F1 score, mean squared error (MSE), and others, depending on the goals of the model. Confusion matrix is commonly used by researchers to assess the effectiveness of the model for classification on infrared images [105], [106], [109], [110]. With this technique, all the important scores can be extracted to represent the data collected to understand the behaviour of their model towards the datasets. To validate their model's performance, researchers also used the method of comparative analysis with other pre-existing models. Pre-trained models such as SqueezeNet, GoogleNet and ShuffleNet were used with the method of transfer learning on same datasets to validate their newly developed network's performance on classifying the infrared images of PV panels based on their health [113]. AlexNet, VGG16, ResNet-18 and Akram's model were used to conduct comparative analysis and it shows better accuracy percentage for their model on PV cell fault classification with faster calculation and prediction speed [110]. Performance metrics to validate the data is also an important step to justify the model's reliability on their accuracy to classify images. Performance metrics allow for the comparison of different neural network architectures, configurations, or techniques. Moreover, it can help to identify whether a neural network model is overfitting or underfitting according based on the training data.

The advantages of these classifiers include their simple architecture, reduced complexity, lesser demand for storage, and quick execution. Their complex design and nonlinearity, which leads to improved accuracy, nonlinear and deep network-based classifiers, like convolution neural networks, offer an advantage in multi-class-based classification. CNNs consist of multiple layers of convolutional and pooling operations that progressively extract features from the input images. Thermal images capture heat distribution patterns, which can be indicative of structural damage or abnormalities. These learned features represent various aspects of the input data, such as edges, textures, shapes, and patterns, which are essential for discriminating between different classes, including damaged and undamaged samples. These extracted features can then be used to differentiate between damaged and undamaged samples. Pre-trained CNN models, such as those trained on large-scale image datasets, provide a valuable starting point for image classification tasks [107], [110]. CNNs can be scaled to accommodate datasets of different sizes and complexities, making them suitable for both small-scale and large-scale image classification tasks.

Based on the literatures, it can be found that the method of transfer learning and developing a new model works efficiently for infrared images. However, the time taken for training and model complexity are among the factors to consider to improve the overall performance of the models. Moreover, the variety of data a model can classify is also an important aspect for model's effectiveness. Most existing models classify infrared images but the ability to capture different types of images such as grayscale images with defects are not represented more in the research previously.

Infrared thermography captures thermal images that reveal hotspots and temperature anomalies caused by lightning strikes, while CNNs process these images to identify patterns, classify damage types, and quantify the severity of faults. Recent advancements have significantly improved the effectiveness of this approach. For instance, enhanced data preprocessing techniques, such as contrast-enhanced grayscale imaging and noise reduction, have optimized thermal image quality. Deep CNN architectures, including transfer learning with models like ResNet and VGG, enable more accurate feature extraction and fault classification.

Expanding datasets with diverse, labeled examples of lightning damage across various panel types and conditions will improve model effectiveness. Lightweight CNNs combining thermal data with visual, ultrasonic, or electroluminescence imaging can enhance accuracy. Predictive maintenance systems, powered by CNN-based insights, could anticipate damage risks, minimizing downtime and repair costs. This synergy of IRT and CNNs is paving the way for smarter, more efficient solar panel monitoring and maintenance.

2.6 Summary

Researchers have widely tested these solar panels for various types of damage. However, the ability to resist damage has not been compared by researchers to know which panel could resist damage well when exposed to certain conditions such as lightning strikes. This comparison would help determine the appropriate type of panels according to the weather conditions in the area. Windy weather and regions highly affected by thunderstorms could use this information to determine that. Besides that, the cost of repairing and replacing the damaged panels could be reduced. This research aims to study the damage intensity of lightning strikes on monocrystalline and polycrystalline panels. Active and passive thermography are commonly used to detect damage to solar panels. Since passive thermography does not require a heating source, many researchers utilized this advantage to examine the panels for damage. This technique has also been applied to unmanned aerial vehicles because the payload will be less with the thermal camera without an excitation source. However, active thermography has shown that the detectability of damages using this technique is equally good as passive thermography. In dark conditions, such as at night or in poor weather conditions, active thermography could detect damage on solar panels. This research would apply active infrared thermography to detect the lightning strike damage on solar panels with the integration of CNN for classification of damage.

CHAPTER 3

METHODOLOGY

3.1 Introduction

This research aims to determine the intensity of damage resistance on two types of solar panels: monocrystalline and polycrystalline. Lightning strike impulse will be generated on the samples with different intensities. This methodology involves three main steps for this research: material preparation, active infrared thermography and data analysis. Figure 3.1 shows the general methodology of this research. The method starts with preparing the solar panel samples. Lightning strike impulses will then be induced in these samples. After that, we carry out the thermography for inspection purposes. Then, the image processing will be carried out to detect the damage from the thermography images. After the experimental work, image classification with the newly developed CNN model will be completed.

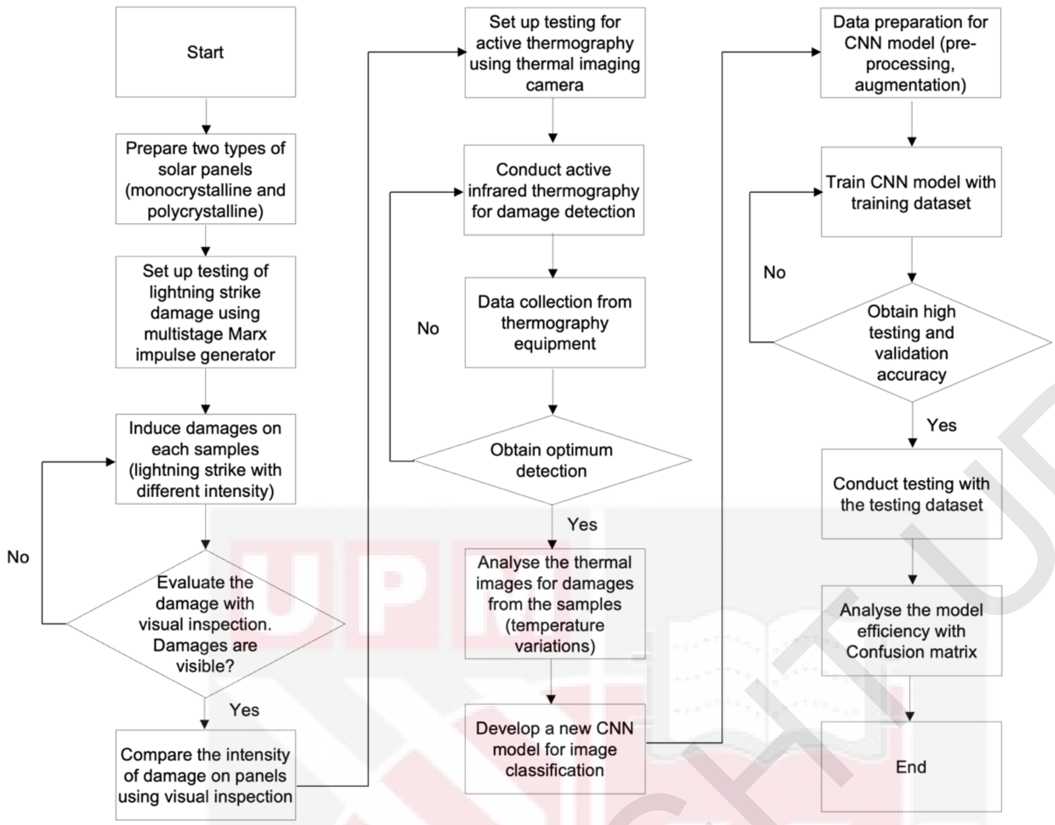

Figure 3.1: The overall methodology of the research

3.2 Sample preparation and specifications

This section discusses the types of samples used in this research, which are the monocrystalline and polycrystalline panels.

3.2.1 Monocrystalline solar panel samples

This research used three monocrystalline solar panels, which are composed of single-crystal silicon as shown in Figure 3.2. Two of these three panels do not have power output, and one does. They were labelled as M1, M2, and M3, respectively.

The panels in Figure 3.2 (A) and (B) are 14.5 x 14.5cm. Their working voltage is 7.4V, and their power is 1.4W. Due to their small size, these panels have a small capacity. This product weighs 85g.

The size of panel in Figure 3.2 (C) is 13.8 x 8.2cm. The working voltage is 5V, and the power is 1.5W. The weight of the panel is approximately 104g. This panel is made of monocrystalline silicon and PET laminate. This panel do have a USB interface as the output.

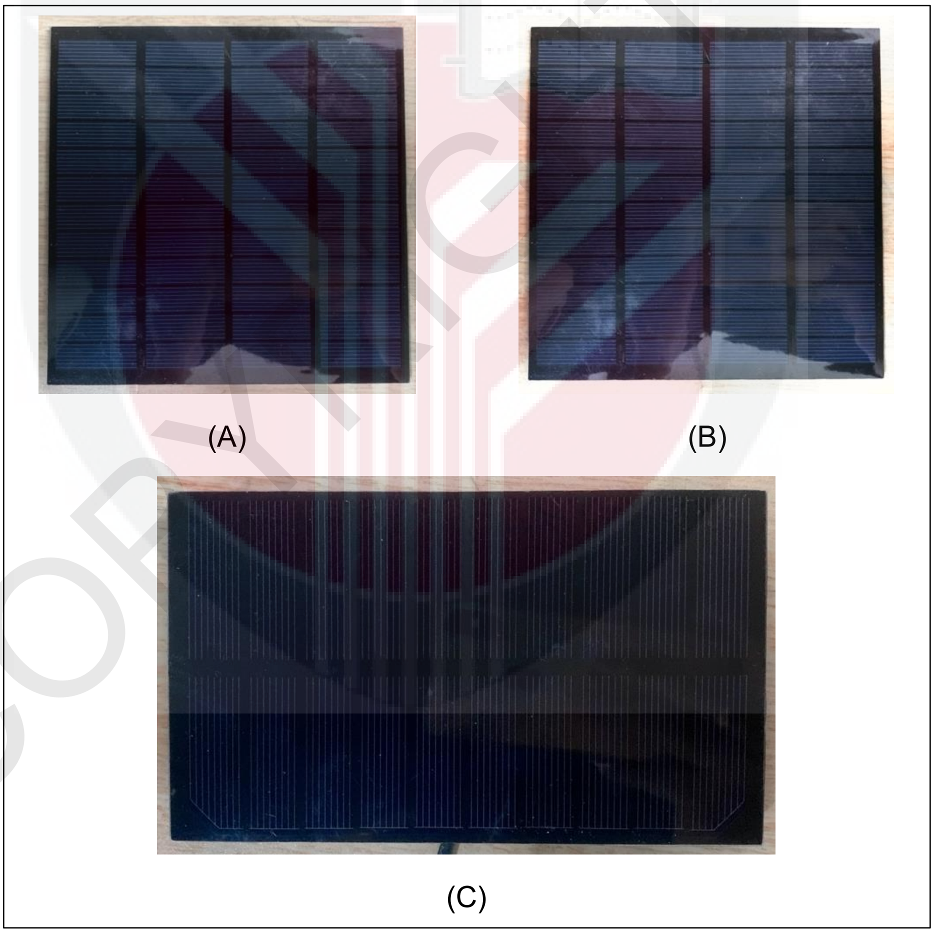

Figure 3.2: Monocrystalline samples, (A) M1 (B) M2 (C) M3

3.2.2 Polycrystalline solar panel samples

Similar to monocrystalline panels, this research used three polycrystalline panels as shown in Figure 3.3. Polycrystalline solar panels are made by melting many fragments of silicon together. Two of these three panels do not have power output, and one does. They were labelled as P1, P2, and P3, respectively.

The panels in Figure 3.3 (A) and (B) are 21 x 16.5cm. They have a working voltage of 12V and a power of 3W. Due to their small size, these panels have a small capacity.

This panel in Figure 3.3 (C) is 13.3 x 7.6cm, has a working voltage of 5V, and has a power of 1.5W. It weighs approximately 104g. The output of this panel is a USB interface.

(A (B) (C)

Figure 3.3: Polycrystalline samples, (A) P1 (B) P2 (C) P3

The samples were separated and it was labelled according to the testing conditions. Since the panels arrived in a good condition, there was only minor cleaning conducted to remove dust on the surface. Both the panels had glossy surface, thus there is not much difference in preparing the samples.

3.3 Experiment on inducing lightning strike damage on samples

This section discusses the method of inducing lightning strike impulses on samples using a Marx impulse generator. It includes all the parameters relevant to this method.

3.3.1 Equipment and setup of sample and impulse generator

A multistage Marx impulse generator induced the lightning strike effect, as in Figure 3.4.

Figure 3.4: The multistage Marx impulse generator

Figure 3.5: The experiment setup (side profile)

The samples were placed on a wooden surface with grounding. Figure 3.5 shows the side profile of the experimental setup. Since this is a high voltage testing, excess electrical charge that could build up on the samples during the test is dispersed using grounding. Inadequate grounding increases the possibility of electrical arcing, which may damage equipment and risk people's safety. Moreover, electrical energy is usually released into the atmosphere when lightning strikes. The test arrangement more closely resembles the circumstances of an actual lightning strike by grounding the samples, improving the test results' accuracy and dependability. The experimental setup is shown in Figure 3.5 and Figure 3.6.

The gap between the metal pointer and the sample is 17.7cm (7 inches). The metal pointer acts as the point where the spark discharges on the panel for the lightning impulse effect. The front profile of the experimental setup, with the metal pointer and the sample, is shown in Figure 3.6.

Figure 3.6: The experiment setup (front profile)

3.3.2 Impulse voltage measurements during the strike

Different impulse voltage intensities were induced to observe the intensity of damage to the solar panels. The experiment started with a 20kV impulse voltage and increased it to 30kV. 30kV was set as the threshold voltage. The threshold voltage was set to identify the point where damage starts appearing on samples by exposing samples to a variety of impulse voltage levels. This threshold voltage gives important information about the electrical insulating qualities of the material and indicates its vulnerability to electrical stress. This research used 30kV, 60kV and 90kV as the impulse voltage for three monocrystalline and three polycrystalline panels. Figure 3.7 shows the lightning strike being induced on the sample.

Figure 3.7: Lightning strike induced on sample

3.3.3 Environmental conditions

This experiment was conducted during sunny days. Rain can introduce moisture into experimental setups, affecting the insulation properties of materials and electrical components. Moisture can increase the risk of electrical arcing, short circuits, and equipment damage. Conducting high-voltage experiments during thunderstorms poses significant safety risks due to the potential for lightning strikes. Lightning is a natural phenomenon involving extremely high voltages and currents, which can cause severe damage to equipment and pose a danger to personnel. Thunderstorms often generate significant electromagnetic interference due to the rapid discharge of electrical energy in the atmosphere. This electromagnetic interference can disrupt experiments by interfering with signal measurements, inducing unwanted electrical currents, or causing equipment malfunctions.

Conductive materials were kept in insulation while conducting this experiment. Conductive materials can distort the electric field around the spark discharge region, leading to non-uniform discharge patterns or altered discharge characteristics. This can affect the accuracy of experimental results. Conductive materials near spark discharge experiments can also pose safety risks, especially if they are not properly grounded or insulated. If conductive materials are not properly insulated or shielded, they may inadvertently create unintended discharge paths or short circuits. Proper shielding and isolation techniques should be employed to minimize interference and ensure reliable results.

Safety precautions were also taken while conducting this experiment. Insulating shoes and gloves were worn to prevent exposure to electrical currents. Helmets were worn to provide protection against head injuries. Earplugs were worn because this equipment generates a high level of noise.

3.4 Infrared thermography for damage detection

This section discusses the infrared thermography method for damage detection on the solar panels. For damage detection on solar panels, passive thermography is commonly used by researchers because heat energy is utilized to convert electrical energy. Moreover, solar panels are exposed to sunlight during the day. However, this research uses active thermography to familiarize a situation with no sunlight, and when passive thermography cannot be carried out.

3.4.1 Equipment and setup of thermal camera

The active thermography for this research used two halogen lamps as a heating source to heat the panels. These halogen lamps were manually controlled by an on/off switch. This research used a tCam-Mini Rev 4 wireless thermal camera board to capture the thermal image. This device has both a Wi-Fi interface and a hardware interface for easier communication with other devices. The thermal camera can capture the temperature difference within an image. Drastic changes in the surrounding temperature will show the defect on the solar panel. The data from this thermal camera will be collected as images. A desktop application, iOS application, simple web server, and Python library are also supported. This device comprises a 160x120 pixel radiometric thermal imaging camera (FLIR Lepton 3.5). It also has a USB interface for power and programming. The experimental setup is portable and built in a wooden case with rollers at the bottom. This makes it easier to experiment with different places. Figure 3.8 shows the experimental setup for infrared thermography.

The environment was set to dark to prevent reflection from the external environment. As an extra precaution, the equipment was covered with black cloth to avoid light. The experiment was conducted at room temperature.

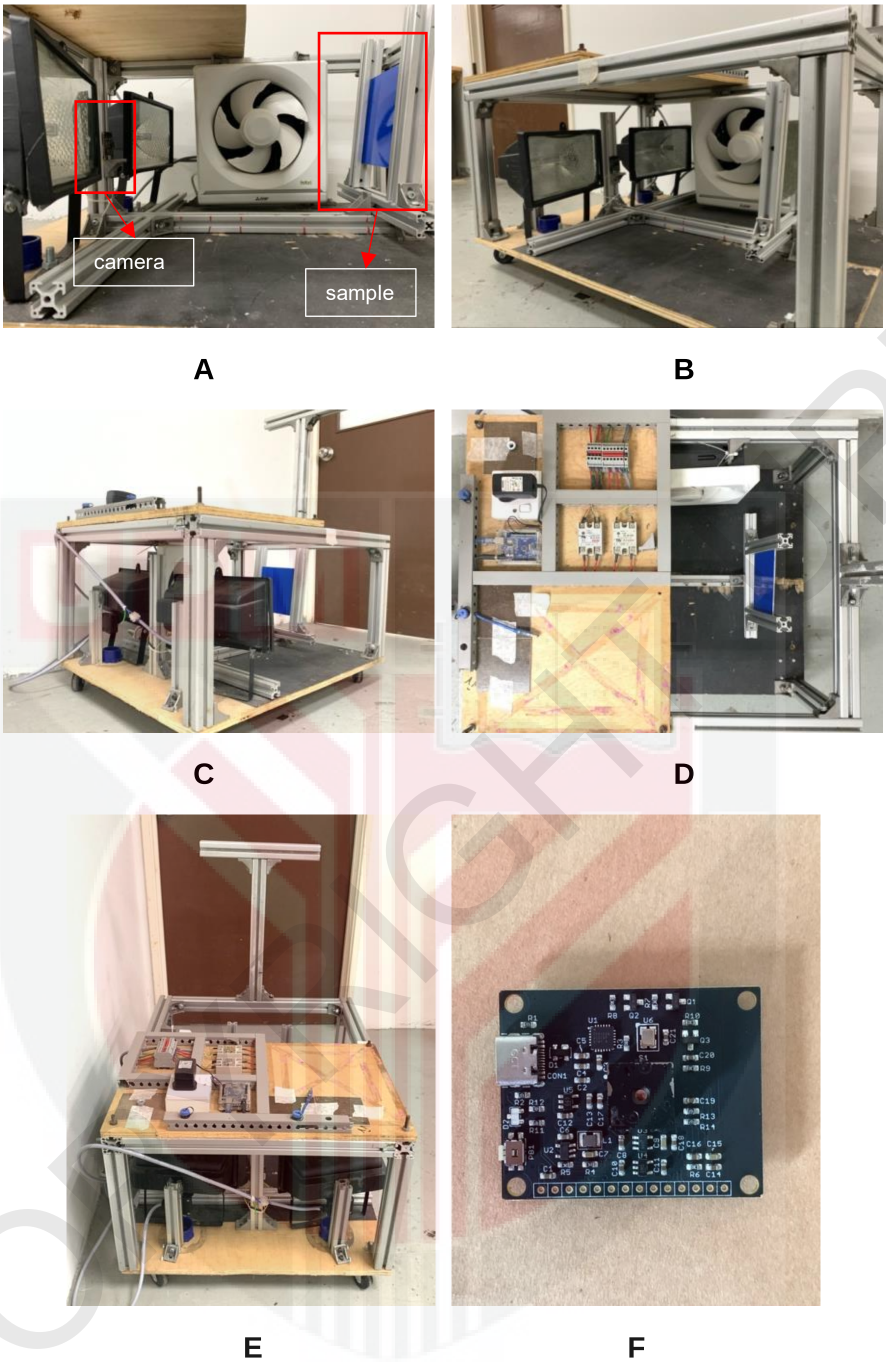

Figure 3.8: (A) Side view of experimental setup (B) Orthogonal view of experimental setup (C) Orthogonal view of experimental (D) Top view of experimental (E) Back view of experimental setup (F) tCam-Mini Rev4 wireless thermal camera board

3.4.2 Heating duration of samples and the distance from the camera

The heating duration for the samples was 15 seconds. After 15 seconds, the halogen lamps were turned off, and the cooling period was 10 seconds. It is a short and quick process because solar panels take a shorter time to heat up and cool down. After the cooling period, the data was collected using the desktop application. The distance between the camera and the sample is 20 cm. The camera was placed closer to the sample because the samples were smaller, and the observation needed to be closer to view the damage on the thermal camera.

3.4.3 Image capturing and storing

The data were captured as video using the desktop application. The images were extracted frame by frame from the video to check for damages. Temperature differences were observed from the images. Markers were placed on the images to show the difference in the temperature of the damage from the samples and the background. Using the desktop application, the colour palette was adjusted according to the temperature range to show more refinement when the temperature difference was small.

3.5 Neural network integration

This section presents a newly developed neural network model for image classification. It includes the network's development method and the data preparation for training and validation.

3.5.1 Neural network model development

A CNN model was developed in MATLAB. This model was developed to classify images of damaged and undamaged samples from infrared thermography. This architecture consists of multiple convolutional layers, max-pooling layers for feature extraction, and fully connected layers for classification. The network aims to achieve higher accuracy in classifying thermal and grayscale images for small damages, such as in this research, than existing pre-trained models. It aims to achieve high accuracy by extracting features from input images and making accurate predictions. This network consists of 90 layers with 97 connections.

The input data consists of RGB and grayscale images with dimensions of 227x227 pixels. The number of channels was changed when processing grayscale images. The input images are normalized using the ‘zerocenter’ normalization method. The use of the zerocenter normalization method helps align the input image values to a mean of zero, reducing input variability and improving model convergence during training.

A total of 28 convolution layers were applied in this model. This architecture is highly capable of extracting hierarchical features, making it well-suited for complex image classification tasks. The height and width of the filter were specified and increased up to 3. It defines the kernels used in the convolutional layer. The use of 3x3 kernels ensures that the receptive field covers more localized image features, enabling the network to detect small-scale damage effectively. The number of filters was expanded and contracted throughout the network. This was carried out to capture different features of the input images. The network started with fewer filters to capture low-level features of the image, such as edges and textures. The expansion of the filter captures more detailed features of the image to learn complex characteristics within an image. After the learning process throughout the network, the number of filters was contracted to capture and recognize important features relevant to this research for the classification of images. This network uses Xavier initializer as the weight initialization method. This method balances the weights so that they neither diminish nor explode during backpropagation, ensuring stable gradient flows across all layers. The biases were initialized using zero initialization to ensure the network starts unbiased and learns relevant offsets during training.

Batch normalization is applied between the convolutional and ReLU layers to normalize the input to the next layer for every mini-batch. It aims to stabilize and speed up the training process. The decay value for moving mean and variance computation was set to 0.1. The constant to add to the mini-batch variance was set to 0.00001. Before normalizing the mini-batch variances, this constant is added to ensure numerical stability and prevent division by zero. ReLU (Rectified Linear Unit) is the activation function used throughout this network. This activation function introduces non-linearity to the network for complex data learning. The hybrid pooling approach is used in this network, where two pooling layers are used: average pooling and max pooling. Alternating between these two pooling methods can provide advantages for both types of pooling. In max pooling, the input is split into rectangular zones, and the maximum of each region is calculated. Meanwhile, average pooling calculates the average from every region. This method helps to capture detailed features from one layer and provides generalised down-sampled representation in another layer. Alternating between max pooling and average pooling creates a balance between retaining prominent features (via max pooling) and smoothing noise (via average pooling).

To prevent overfitting, dropout regularization with a dropout rate of 0.3 is applied before the fully connected layer at the end to promote the network's ability to generalize across unseen data. The classification layer is the final layer of this network to classify the damaged and undamaged images. It generates predictions based on the features extracted throughout the preceding layers. SoftMax activation function was applied in the output layer, representing the probability distribution of the classes. The network output shows the probabilities for each class in a predefined set of categories. The highest probability is selected as the predicted class for the input data. Despite the depth (90 layers), techniques like batch normalization and optimized weight initialization prevent common pitfalls like vanishing gradients, ensuring stable and efficient training. The network's flexibility in handling multiple image formats ensures its applicability to diverse datasets, even in scenarios where only one format is available. Figure 3.9 shows the complete architecture of the newly developed network model.

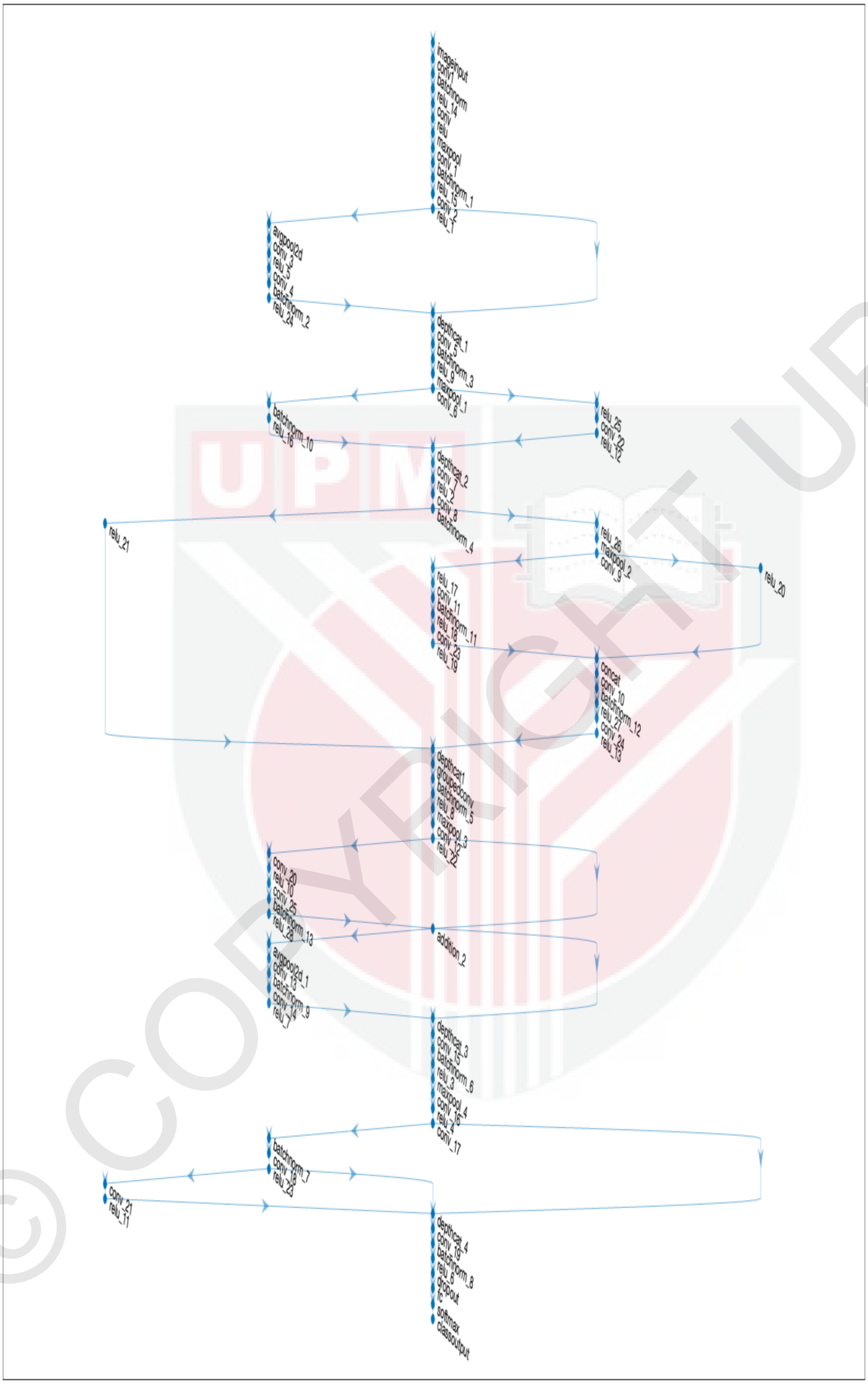

Figure 3.9: Architecture of the newly developed convolutional neural network

3.5.2 Preparation of training and validation dataset

Before training, the input images were cropped from the original images to fit the panel with a full frame. Three datasets were created for this research. The first dataset uses the original thermal images obtained from the thermography. The second dataset comprises images that were converted to grayscale. This conversion was done using MATLAB. It was converted using 0.2989 * R + 0.5870 * G + 0.1140 * B, where R indicates red, G indicates green, and B indicates blue. To refine the details, the third dataset uses contrast-adjusted images processed from the grayscale images. This process was also done in MATLAB. The contrast limits were set to 0.55 to 1.

400 images were prepared for every data set for neural network training, validation, and testing. 40% of these images were allocated for training, 30% for validation, and 30% for testing. This research uses the holdout validation technique, where the datasets are split into training and testing. The images for testing were not used in training to ensure the reliability of the network performance. This technique is suitable for this research because of the limited data.

A Stochastic Gradient Descent with Momentum (SGDM) optimizer with an initial learning rate of 0.01 was used in the training process. This learning rate is to have a stable update on the training process without divergence or convergence. The number of epochs used to train this network was 20, with a mini-batch size of 35.

3.6 Summary

This methodology includes thermal imaging technique to detect the temperature anomalies caused by damages such as dents, bubbles and hotspots. The thermal patterns on the surface of the panels are observed and irregularities are detected while conducting thermal imaging. To validate the data obtained, image preprocessing techniques were applied, ensuring the thermal anomalies are distinguishable regardless of the panel type.

Smaller size panel allow for a more controlled and precise testing setup, minimizing external factors such as high voltage impulse and temperature distribution, which could affect the results. It requires less infrastructure for testing, making it feasible to conduct multiple trials under varying conditions. The selected voltage intensities simulate varying degrees of lightning strikes. These values were chosen to progressively understand the damage mechanisms and avoid overloading the panels in initial tests. While it is acknowledged that natural lightning can reach much higher voltages, the focus of our study was to investigate the effects of varying intensity levels within a controlled and manageable range. The voltage intensities of 30kV, 60kV, and 90kV were chosen as initial steps to explore the behavior of solar panels under electrical stress. These levels provide a safe and controlled environment to observe the fundamental damage mechanisms and material responses.

The implementation of active thermography serves as the primary method for data acquisition. The thermal camera's resolution is lower, resulting in an inability to capture high-quality images of the samples. However, the captured images could show the samples' damages even with said quality. To make the results even more reliable, the images were also processed into two other forms: converting them to grayscale and adjusting their contrast. Certain parameters were standardised to ensure proper defect detection on samples. These parameters are the heating duration, distance, the surrounding environment, and temperature.

A CNN was developed for data analysis. While building the network, the convolutional filters were adjusted according to the architecture to examine the ability to capture the features effectively. Many filters would make the network heavier and more difficult to process, consuming a lot of time. Meanwhile, fewer filters would cause the network not to capture the required features effectively. Thus, several trials are needed to reach a point where the network can capture the feature properly and efficiently. Moreover, the datasets were imbalanced, with more images in the undamaged class than in the damaged class. However, training and testing were carried out using these data. This scenario can represent real-world situations where imbalanced classes are common.

CHAPTER 4

RESULT AND ANALYSIS

4.1 Overview

This section presents the research findings, including the intensity of lightning strike damage on two types of solar panels of different compositions. This section also focuses on employing neural network techniques to address this classification task, aiming to improve efficiency, accuracy, and reliability compared to existing models. The results of our study on the classification of damaged and undamaged samples using a newly developed CNN were presented. A detailed analysis of the confusion matrix was included, followed by a discussion of the performance metrics and their implications.

4.2 Experimental results of induced lightning strike on samples

This section presents the experimental results, including an evaluation of the solar panels' visible damage and a comparison of the panels with the lightning strike intensity.

Lightning strikes were induced on the solar panel samples. For this research, Marx’s impulse generator was used. This multistage impulse generator comprises 10 stages to generate high impulse voltage on samples. The impulse voltage used for this research is 30kV, 60kV and 90kV. There were 6 samples were used to test for this voltage: 3 monocrystalline and 3 polycrystalline panels. Sample M1 & P1 were tested for 30kV impulse voltage. Sample M2 & P2 were tested for 60kV impulse voltage and sample M3 & P3 were tested for 90kV impulse voltage. For samples M1 & P1, the impulse voltage was increased from 20 kV to 30 kV with an increment of 2 kV until it damaged the panels to get the base parameters. From this basic testing, the other impulse voltage parameters were determined to be continued with other panels.

4.2.1 Evaluation of visible damages on samples

All these panels showed different behaviours when tested for different impulse voltages. The panels were looked at for visible damage on the surface. For monocrystalline, sample M1 showed no visible damage when exposed to 30kV impulse voltage. Meanwhile, sample M2, which induced 60kV impulse voltage, had minor peeling at the edge of the panel but no other damage on the surface. However, sample M3 had no visible damage when exposed to 90kV impulse voltage.

For polycrystalline samples, P1 showed the formation of small bubbles on the panel's surface after being exposed to 30kV impulse voltage. A minor dent with 0.2 cm and small bubbles on the surface were noticed on sample P2, which induced 60kV impulse voltage. However, sample P3 shows no visible damage after exposure to 90kV impulse voltage.

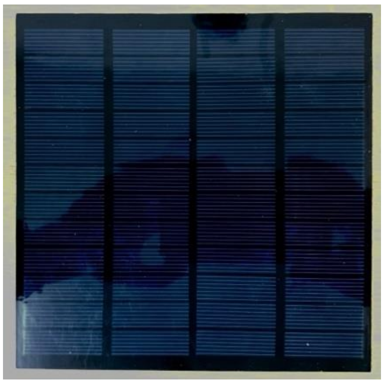

Figure 4.1: Damaged M1 sample (30kV)

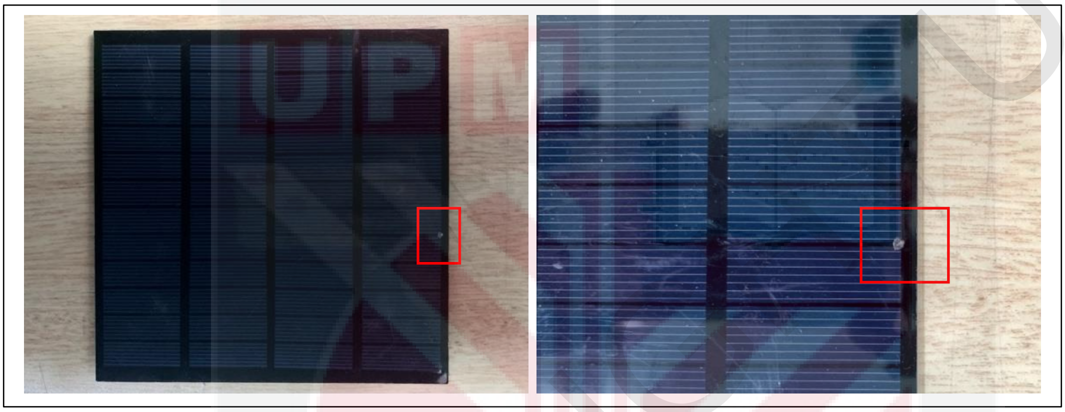

Figure 4.2: Damaged M2 sample (60kV)

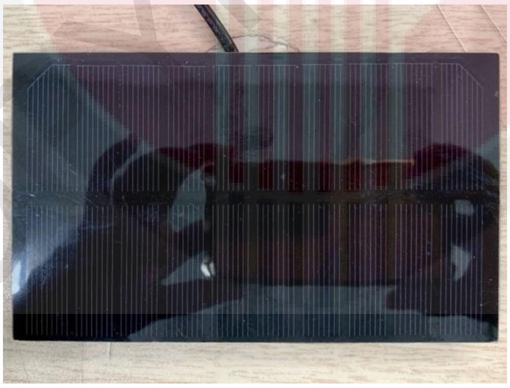

Figure 4.3: Damaged M3 sample (90kV)

Figure 4.4: Damaged P1 sample (30kV)

Figure 4.5: Damaged P2 sample (60kV)

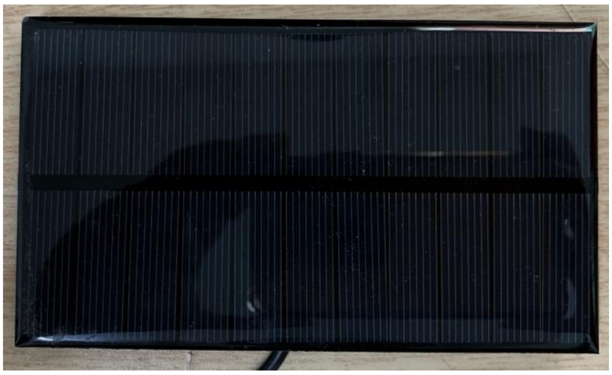

Figure 4.6: Damaged P3 sample (90kV)

4.2.2 Comparison of two types of samples for visible damages

When comparing monocrystalline panels, the panels tested for 60kV show minor visible damages, and the panels tested for 30kV and 90kV do not show any visible damages. Comparing the polycrystalline panels, both panels tested for 30kV and 60kV show visible damages on their panels, such as bubbles and dents. However, the panel tested for 90kV does not show any visible damage. When comparing the intensity of the voltage on the panels, for 30kV impulse voltage, the monocrystalline panel does not show visible damage. Still, bubbles have formed on the surface of the polycrystalline panel. Meanwhile, for 60kV impulse voltage, minor visible damage was observed on the monocrystalline panel, and a dent formation was observed on the polycrystalline panel. However, both panels tested with 90kV impulse voltage show no visible damage.

The key difference that was observed visibly between those panels are monocrystalline panels had lesser damages compared to polycrystalline panels. Only minor peeling was observed on monocrystalline panel, but for polycrystalline panels there were bubbles and dent formed when exposed to high voltage impulse.

Since the panels tested for 90kV do not show visible damages or changes, it is assumed as an outlier. There are a few possibilities for this occurrence. The grounding of the panels could be a reason. All the panels were grounded before experimenting for safety reasons and to demonstrate a more practical approach to this research, as most of the panels out in real-life situations are grounded. This could have caused the panels to have prevented the damage of induced lightning strikes. To explain the other cases where the panels have been damaged despite being grounded, it is important to note that grounding does not guarantee complete protection from lightning strikes, but also other measures, such as surge protection devices and appropriate design, might be helpful to prevent these cases. Besides that, insufficient grounding could damage the panel because it cannot dissipate the electrical energy effectively. From this visual observation, it can be noticed that the structure of monocrystalline panels is more capable of enduring minor lightning impulses than polycrystalline panels.

4.3 Experimental results of infrared thermography on samples after lightning strike damage

This section presents the results from infrared thermography and discusses the damage to the thermal images obtained with temperature variation. It also compares the damages on the two types of panels that could be observed through the thermal images.

4.3.1 Parameters of the duration of heating and distance of samples from an infrared camera

The samples were heated using halogen lamps before being exposed to a thermal camera for infrared thermography. The samples were heated for 10 seconds with two halogen lamps. The heated samples were then carried out infrared thermography using tCam-Mini with a thermal imaging camera (FLIR Lepton 3.5). The distance of the samples from the thermal camera is 20 cm. The output is then captured as a video with a wireless connection until the temperature cools down to observe the temperature variations on the samples.

4.3.2 Evaluation of temperature variations on samples

4.3.2.1 Monocrystalline panels

Sample M1

For M1, it does not show any damage under the infrared camera. However, the sample showed varied temperature distributions. This is due to the emissivity factor. Emissivity is the measure of an object's ability to emit infrared energy. Emitted energy indicates the temperature of the object. Usually, a shiny surface has an emissivity value of 0 and a black surface of 1. The varied temperature distribution is caused by the reflected temperature of the thermal

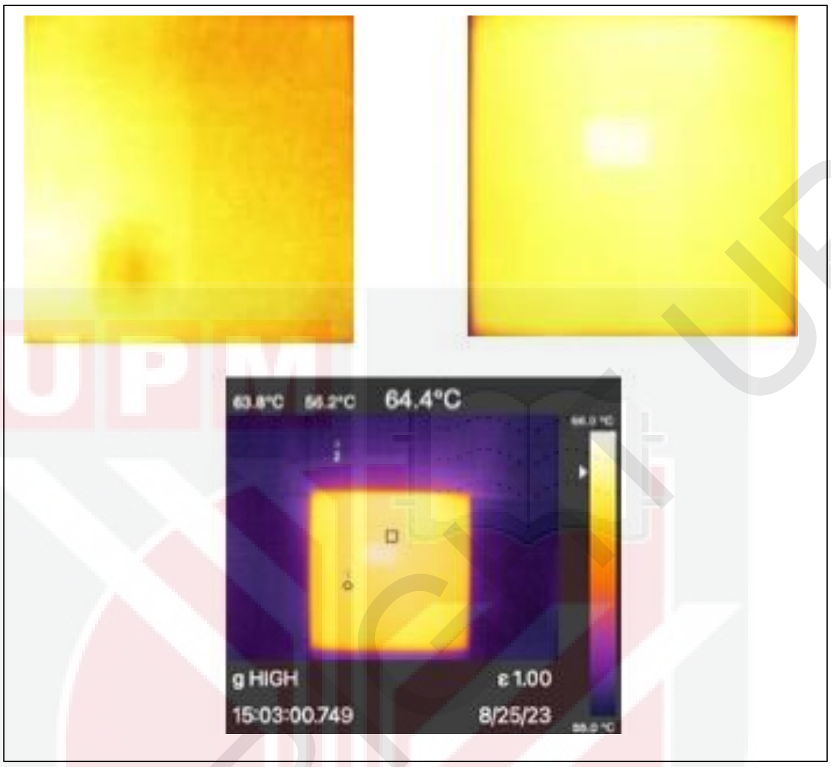

Figure 4.7: Thermal images of M1 sample.

camera on the solar panel. Low emissivity indicates that it reflects the heat more than material with higher emissivity. The surface of the solar panel is black, but it is also a reflective material. The background shows 56.2°C and the panel shows 63.8°C. A higher temperature is recorded at the center at 64.4°C due to the thermal camera's reflection on the panel.

Sample M2

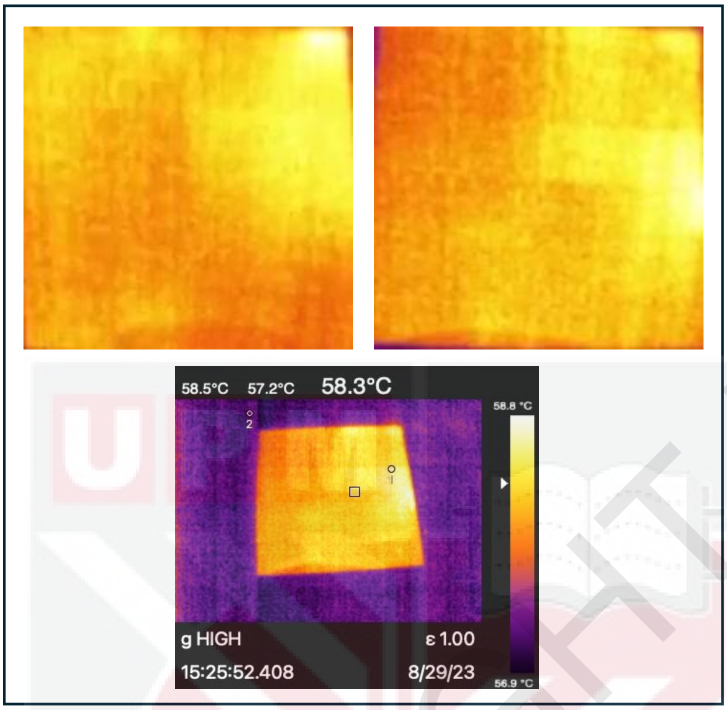

Figure 4.8: Thermal images of M2 sample.

In the infrared thermography for M2, no distinct temperature variations are observed on the infrared images. Similar to M1, slight temperature variations exist, but it does not indicate damage. The background shows 57.2°C, and the panel temperature ranges from 58.3°C to 58.5°C with a 0.2°C difference, which is not a major variation to indicate damage.

Sample M3

The infrared thermography shows no damage or temperature variation for M3. The temperature remains constant throughout the panel's surface. The background shows 60.2°C, and the panel shows 62.0°C.

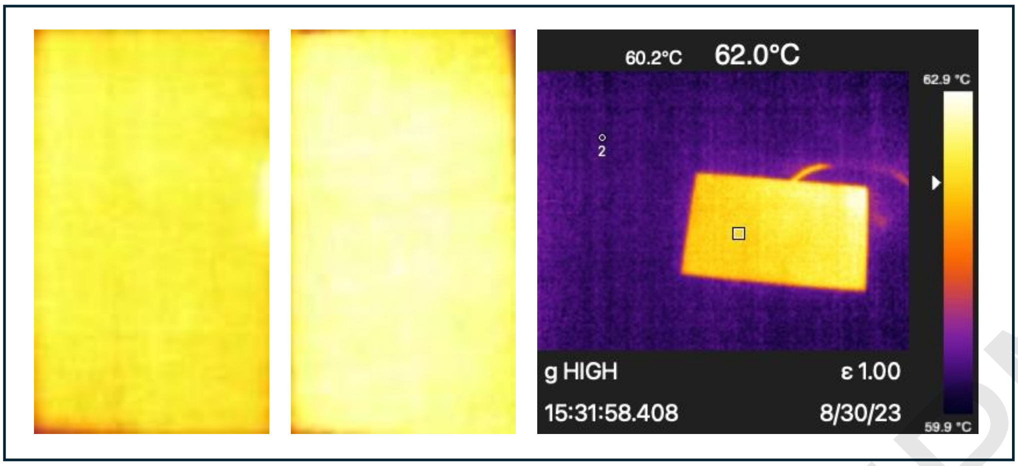

Figure 4.9: Thermal images of M3 sample.

4.3.2.2 Polycrystalline panels

<u>Sample P1</u>

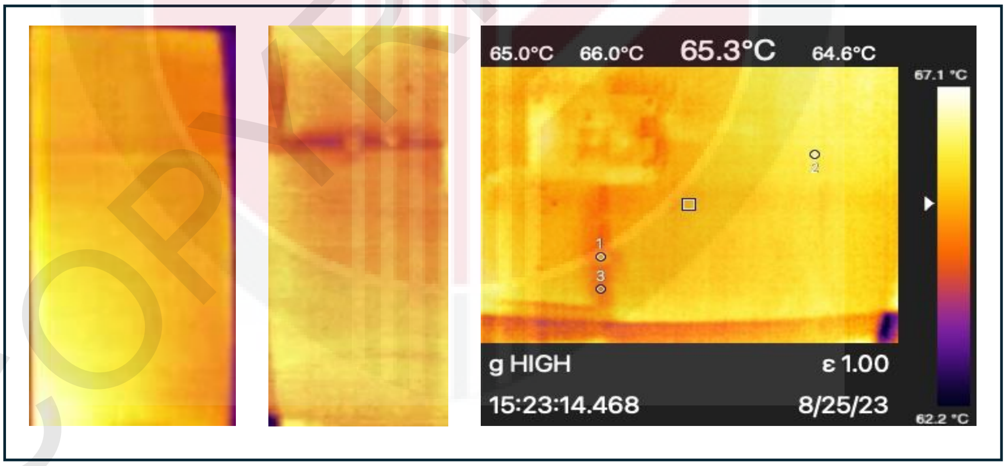

Figure 4.10: Thermal images of P1 sample.

The infrared images of P1 show defects. The bubbles observed during the visual inspection can be seen through infrared thermography. The bubbles are significantly smaller but can be observed with a thermal camera at a different temperature than the background. The defect area shows temperatures of

65.0°C and 64.6°C, which are lower than the background at 66.0°C and 65.3°C at different panel regions.

Sample P2

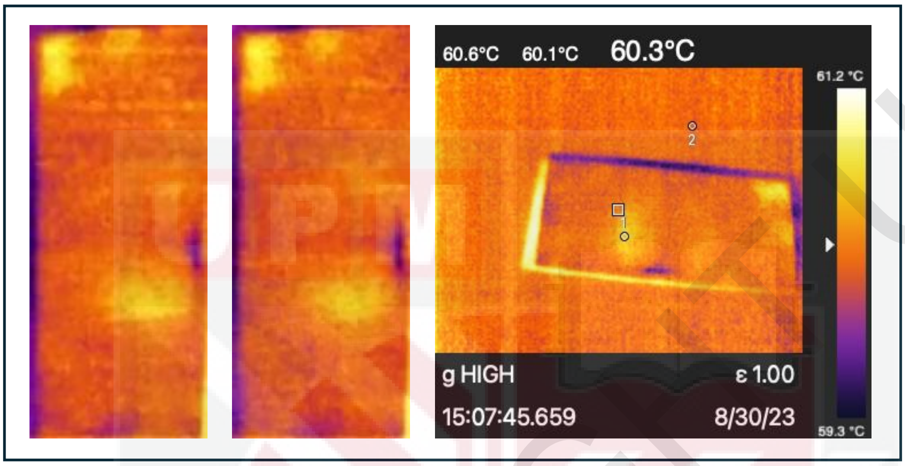

Figure 4.11: Thermal images of P2 sample.

The infrared images show a major temperature variation for P2. As mentioned earlier, a small dent was observed, and the infrared image shows a higher temperature at the dent. The background temperature is 60.1°C, and it shows 60.6°C at the dent.

Sample P3

For P3, no damages were observed in the infrared images. The panel shows 65.5°C and the background temperature is 60.6°C.

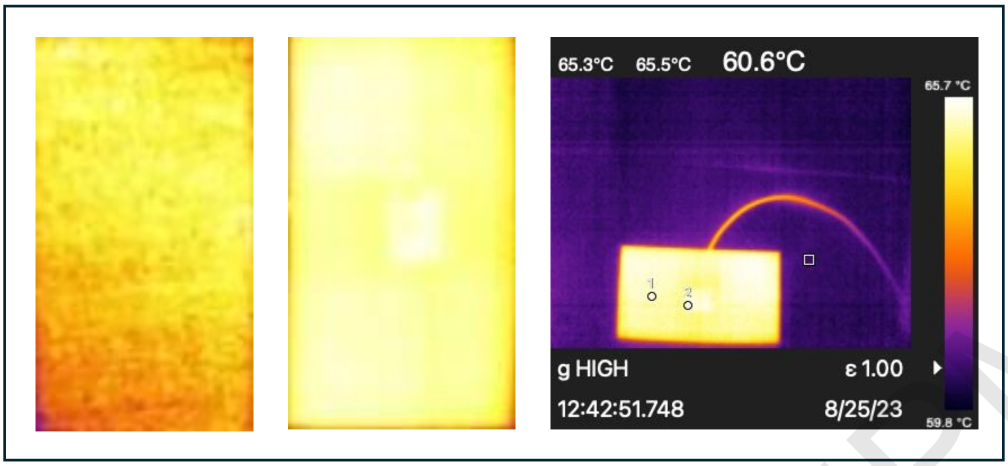

Figure 4.12: Thermal images of P3 sample.

4.3.3 Comparison of two types of solar panels based on infrared images

Observing the infrared images shows that polycrystalline panels are more damaged by lightning strikes than monocrystalline panels. Polycrystalline panels show damage, such as bubbles and dents, on infrared images due to temperature variation on the surface. The bubbles had lower temperatures than other surface parts, with approximately a 1°C difference in sample P1. Meanwhile, the dent observed in sample P2 shows a higher temperature at the defect than another part with a 0.5°C difference. The surface temperature distribution is usually disrupted when there is abnormality on the surface, such as damage. Bubbles showing cooler regions suggest insulation effects or air entrapment disrupting heat conduction. Dents showing warmer regions indicate potential localized heat concentration due to structural deformation or increased resistance. This is the cause of the rise and drop of temperature on the surface of these polycrystalline panels. Sample M2 was observed for minor peeling on the surface for visual inspection but is not visible on the infrared camera. This might be due to the small and shallow damage to the surface compared to bubbles and dents. Several uneven temperature distributions are observed on the panel due to the emissivity factor. The environment was set to dark to maximize the accuracy of the result, but due to the surface reflection of the panel, uneven temperature is observed in certain instances. Infrared thermography effectively detects visible damages like bubbles and dents, but smaller or superficial damages (e.g., peeling) might go undetected.

4.4 Neural network classification for damaged samples

4.4.1 Training, validation and testing datasets from the samples

The data from the thermal camera were separated into training, validation and testing sets. A total of 400 images were retrieved from the videos that were captured using the thermal camera. These videos were then processed to retrieve images frame by frame to maximize the total number of images to train the neural network algorithm. These images were segregated as 40% for training, 30% for validation and 30% for testing. The images for training and validation were stored in separate files from the testing data. The training and validation data were randomized during the training process to avoid overfitting and underfitting.

Three datasets were used for this analysis, which were sourced from the same thermal camera. The first dataset consists of raw images from the thermal camera without processing. The images were just implemented into the neural network algorithm as how it was. The second dataset consists of images from the thermal camera, which was converted into grayscale. Grayscale images are well known for damage detection. This conversion was made to observe the changes in accuracy for the image classification method with the neural network algorithm. The third dataset consists of grayscale images, which were adjusted for contrast to observe the damaged parts better. The contrast limits were set to 0.55 to 1.0 based on the grayscale images we obtained. The conversion of grayscale images and the contrast adjustment were made in MATLAB.

4.4.2 Classification of damaged and undamaged samples

Accurately classifying damaged and undamaged samples is important across various industries. A new CNN architecture was developed to classify 3 types of images: thermal, grayscale, and contrast-adjusted.

This analysis used the Confusion matrix method to analyze the effectivity of the neural network algorithm. A few interpretations were calculated after obtaining the classification results. The accuracy, error rate, sensitivity, specificity, precision and F1 score are among them. Accuracy measures the frequency of the correct prediction of the classification. Error rate calculates the misclassification rate. Sensitivity is also referred to as the true positive rate, which measures the proportion of actual positive cases that are correctly identified by a classifier. A high sensitivity indicates that the classifier effectively recognizes positive cases, while a low sensitivity suggests that the classifier frequently misses positive instances. Specificity is the false positive rate, which measures the proportion of actual negative cases that are incorrectly identified as positive by a classifier. A high specificity indicates that the classifier is less specific and is prone to incorrectly labeling negative instances as positive. Precision measures the proportion of correctly predicted positive instances (true positives) among all instances predicted as positive by the classifier. The F1 score is a single metric that reflects the overall performance of a binary classifier, considering both its precision and sensitivity. A higher F1 score indicates that the classifier is working effectively.

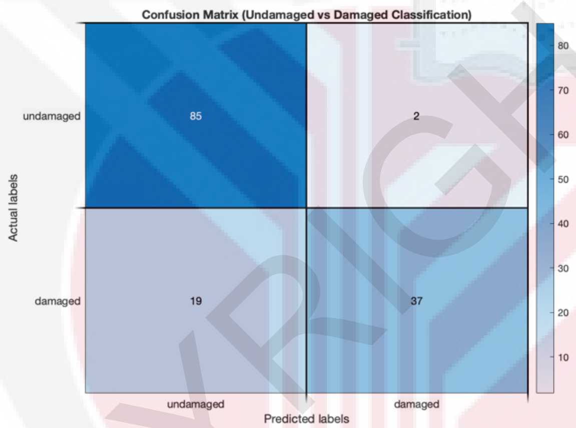

Figure 4.13: Confusion Matrix of thermal images.

According to the Figure 4.13, 85 out of 104 were correctly classified as undamaged, and 37 out of 39 were classified as damaged. 19 images of undamaged samples were incorrectly classified as damaged, and 2 images of damaged samples were incorrectly classified as undamaged. The model's overall accuracy is 85.31%, indicating correctly classified samples. The model's precision, sensitivity, and specificity are 81.73%, 97.70%, and 66%, respectively. The F1 score is 89%, indicating the model's effectiveness on thermal images.

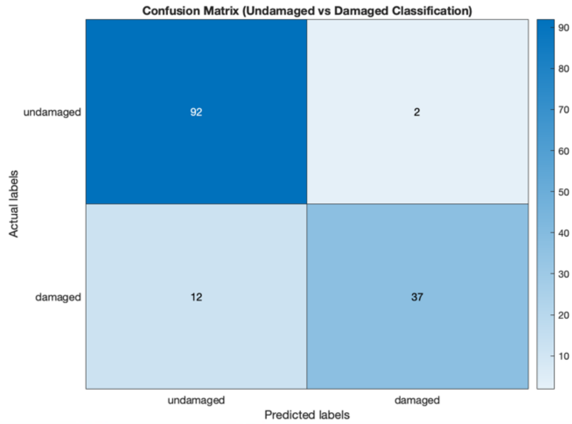

Figure 4.14: Confusion Matrix of grayscale images.

According to the Figure 4.14, 92 images out of 104 were correctly classified as undamaged, and 37 images out of 39 were classified as damaged. 12 images of undamaged samples were incorrectly classified as damaged, and 2 images of damaged samples were incorrectly classified as undamaged. The model's overall accuracy is 90.21%, which is higher than that of the other two types of images. The model's precision, sensitivity, and specificity are 88.46%, 97.87%, and 75.51%, respectively. The F1 score is 92.93%, indicating the model's effectiveness on thermal images.

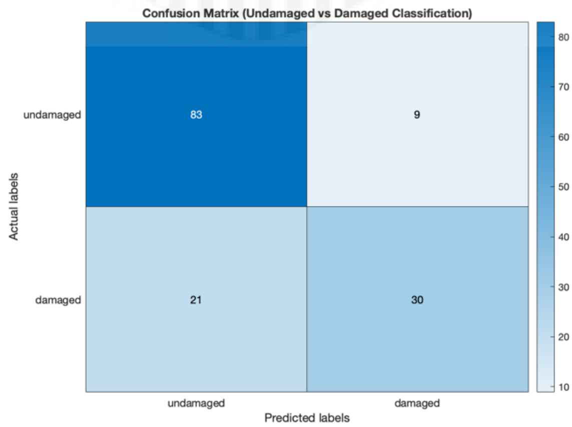

Figure 4.15: Confusion Matrix of contrast-adjusted images.

According to the Figure 4.15, 83 images out of 104 were correctly classified as undamaged, and 30 images out of 39 were classified as damaged. 21 images of undamaged samples were incorrectly classified as damaged, and 9 images of damaged samples were incorrectly classified as undamaged. The model's overall accuracy is 79%, which is lower than the other two image types. The model's precision, sensitivity, and specificity are 79.81%, 90.22%, and 58.22%, respectively. The F1 score is 84.69%, indicating the model's effectiveness on thermal images, which is comparatively lower than that of other types of images.

The proposed model achieves more than 79% accuracy for the three types of images. The error rate shows less than 20% for all types of images. The F1 score for all three types of images is more than 0.84. This result demonstrates that this architecture could effectively classify the damaged and undamaged samples for all types of images used in this research. The visual representation of the confusion matrix shows a balanced distribution of true positives and true negatives with few instances of misclassifications. The interpretation of the confusion matrix reveals that while the model demonstrates high overall percentages for accuracy, precision, sensitivity, specificity, and F1-score, improvement is still needed. The false positive and false negative rates indicate potential weaknesses in the model’s ability to classify undamaged and damaged samples.

4.4.3 Comparison with various algorithms of neural networks for accuracy

The computational performance and complexity of CNNs vary. Different CNN designs may exhibit varying degrees of performance on certain tasks and datasets. By comparing their performances, researchers can better understand which designs are more appropriate for specific applications. Certain architectures may use less computational power or parameters to obtain performance that is equivalent to or better than others. Selecting the most effective model for implementation in situations with limited resources or real-time applications is made easier by being conscious of these variations. New CNN architectures frequently present novel design ideas or architectural advancements. The field can uncover breakthroughs and developments that motivate further study and development by comparing these new architectures with existing ones. Besides that, identifying the advantages and disadvantages of various CNN designs opens the opportunity to investigate methods such as transfer learning, which applies the knowledge from trained models to untrained tasks or domains.

This research used three CNN algorithms for comparison analysis: GoogleNet, Squeezenet and EfficientNet-b0. It is well known that all these three architectures were built for image classification tasks. They also focus more on minimizing computational resources to achieve high performance. Notably, these three architectures have innovative designs to address specific challenges in deep learning. SqueezeNet invented the Fire Module to minimize model size without affecting accuracy [119]. The inception module from GoogleNet was designed to efficiently capture features at various scales [120]. EfficientNet-b0 created compound scaling to improve performance using fewer parameters [121]. Other important variations are presented in Table 4.1.

Table 4.1: Comparison of pre-trained neural network architectures

	SqueezeNet	**GoogleNet**	**EfficientNet**
No of layers	18	22	66
Architecture	Fire module	Inception module	Compound scaling method
Model size	Reduced model size [119]	Moderate	Smaller
Accuracy (based on ImageNet)	56 [119]	69.8 [120]	76.3 [121]
Inference speed	Fastest	Slowest	Slower than SqueezeNet, faster than GoogleNet

Large-scale datasets such as ImageNet, including millions of labelled photos in hundreds of categories, are used to train pre-trained CNN models. These pre-trained models greatly reduce the time and computational resources needed to train a model from scratch. The learned feature representations from pre-trained models can be reused using transfer learning, as they are frequently transferable to other tasks and datasets. Regularizing the learning process through transfer learning results in better generalization of new data. According to Table 4.1, EfficientNet-b0 shows a higher accuracy rate with the ImageNet dataset, and SqueezeNet has the lowest accuracy rate, at only 56 %. However, the inference speed shows that SqueezeNet is the fastest among all three architectures. The number of computations and the complexity of the architecture could also contribute to this factor.

In this research, three types of datasets were used. Among them are the original images from infrared thermography, images converted into grayscale, and images adjusted for their contrast in grayscale. This analysis investigates the type of image that can be classified efficiently using these CNN algorithms and identifies the best algorithm for infrared images specific to this research. The optimization algorithm for this training was the SGDM optimizer with an initial learning rate of 0.001. The weights of the newly added convolution layer were increased to 10 to improve the model's performance and minimize the loss function. The number of epochs used to train these networks ranges from 15 to 30, depending on the adaptability of the network to the images based on training and validation data in the initial cycle.

According to the validation accuracy obtained from the training process, all 3 comparative architectures show more than 94%. EfficientNet-b0 has higher validation accuracy for thermal and grayscale images, and it is important to note that this model has deeper layers than others. However, despite having fewer layers, the newly developed model has higher accuracy overall. This highlights the importance of model simplicity in fostering better generalization. This analysis used the Confusion matrix to analyze the effectivity of the neural network architectures with parameters such as accuracy, error rate, sensitivity, specificity, precision and F1 score. These parameters are presented in Table 4.2.

Table 4.2: Comparison of Confusion Matrix scores

Image type	SqueezeNet	GoogleNet	EfficientNet-b0	Developed network
Accuracy (validation)				
Original	97.33	94.67	100	100
Grayscale	98.67	98.33	98.67	100
Contrast adjustment	97.33	100	98.67	98.67
Accuracy (testing)				
Original	74.83	64.34	86	85.31
Grayscale	90.91	91.61	91.61	90.21
Contrast adjustment	85.31	74.83	74.83	79.02
Error rate				
Original	25.17	35.66	13.99	14.69
Grayscale	9.09	8.39	8.39	9.79
Contrast adjustment	14.69	25.17	25.17	20.98
Sensitivity (True positive rate)				
Original	66.35	51.92	84.62	97.70
Grayscale	100	100	100	97.87
Contrast adjustment	90.38	66.35	66.35	90.22
Specificity (False positive rate)				
Original	97.44	97.44	89.74	66.07
Grayscale	66.67	69.23	69.23	75.51
Contrast adjustment	71.79	97.44	97.44	58.22
Precision				
Original	98.57	98.18	95.65	81.73
Grayscale	88.89	89.66	89.66	88.46
Contrast adjustment	89.52	98.57	98.57	79.81
F1 score				
Original	79.31	67.92	89.80	89.01
Grayscale	94.12	94.85	94.85	92.93
Contrast adjustment	89.55	79.31	79.31	84.69

When all these algorithms are compared to the types of images tested, SqueezeNet produces a great output on contrast-adjusted images compared to the other types of images. GoogleNet shows more promising results on grayscale images than on other types of images. Meanwhile, EfficientNet-b0 works better on thermal and grayscale images than contrast-adjusted images. It is important to note that GoogleNet has shown less accuracy than other algorithms, with only 64.34% for original images and 74.83% for contrast-adjusted images. Moreover, it has also shown a higher error rate with 35.66% and 25.17% for original and contrast-adjusted images, respectively. Although it has performed well with grayscale images, it performs the opposite for other images. For EfficientNet-b0, the performance on original and grayscale images is efficient, but the performance on contrast-adjusted images is unsatisfactory, with a 25.17% error rate and 66.35% sensitivity.

Comparing the pre-trained network to the newly developed network, the developed network works optimally on all the images. The percentage for all the parameters is closer to the best of the three architectures. Unlike other architectures, the error rate is less than 20% for all types of images, which exceeds and rises to 35%. The sensitivity rate for this architecture is more than 90%, which allows it to detect true positive rates effectively. Moreover, the F1 score for all 3 types of images is above 83%, indicating that the classifier is working effectively. Comparing these architectures, EfficientNet-b0 performs well on two types of images: grayscale and original images. However, considering the overall performance for classifying all three types of images, the newly developed network could classify the images effectively with good F1 scores and lower error rates.

Meanwhile, comparing the types of images for neural network algorithms based on this analysis, grayscale images work as a good image dataset compared to other types of images. The accuracy and F1 score are higher in all models than in other image types. The error rate is also the lowest, at less than 10%, for all models. Grayscale images contain only one channel, whereas coloured images contain 3 channels. This dimensionality reduction could reduce the complexity and lead to faster convergence and better performance. Another important factor is the noise in the image is also less than in colored images. A high-contrast image is also on grayscale, but the performance is worse than on grayscale. This might be due to a loss of information on the other parts of images during training, which might have caused poor performance. The models might not be able to capture the information of the whole image. Sometimes, the noise patterns interfere with the intended features, making the models sensitive to irrelevant features.

From this analysis, it can be understood that different networks work differently on different types of images. The choice among these architectures depends on the specific requirements of the task, including computational constraints, accuracy demands, and deployment environments. Certain factors could cause these architectures to perform poorly on the images. The image complexity is a factor for poor performance. It might need to be better represented in the training data, where the patterns and details are difficult for the architecture to recognize and capture. The quantity of training data could have also contributed to this, as there was a limited amount of data, and diversity has also become a constraint for the architectures to perform well.

Another important point to consider is the class imbalance in the training dataset, where one class is overrepresented, which could have caused the networks to perform unsatisfactorily. This comparison underscores the trade-offs between model complexity, computational resources, and performance, providing valuable insights for informed model selection and deployment.

The depth and complexity of the architecture is one of the factors influencing their effectiveness. SqueezeNet has the most efficient architecture compared to EfficientNet-b0 and GoogleNet with minimal parameter count. Complex architectures takes longer processing time and cause overfitting which might result in misleading predictions with higher error rates. In this analysis, it can be observed that at certain image datasets, the error rate was more than 25%. Feature extraction method is also another key factor contributing to the performance of the architecture. SqueezeNet's compact design enables it to generalize well to unseen data, making it robust for small datasets with limited variations in damage types. EfficientNet-b0's compound scaling method ensures consistent performance across datasets with varying complexities, making it adaptable for varying types of image datasets as it performed well on the datasets for this research with good accuracy.

4.5 Summary

The results show that lightning strikes could damage the solar panels at different rates, given their intensity and composition. From the visual inspection and infrared thermography, it can be observed that monocrystalline panels have higher durability against lightning strike damage compared to polycrystalline panels. The monocrystalline panel shows minor damage on the panel with 60kV impulse voltage, and polycrystalline panels show damage on both 30kV and 60kV impulse voltage. This study also investigated the classification of damaged and undamaged samples using a neural network approach. The newly developed model demonstrated good performance in the classification, achieving high accuracy, precision and F1 score for all types of datasets, unlike other pre-trained models, which perform excellently on one or two datasets. Besides that, the classification of grayscale images shows strong performance on all neural network models. The interpretation of the confusion matrix provides detailed insights into the model's strengths and weaknesses. Despite having higher true positive and true negative rates, false positive and false negative rates suggest that the model can be refined further.

The research highlights the need for enhanced panel designs, particularly for polycrystalline panels, which were found to be more susceptible to lightning-induced damage. Improving material selection and structural design to mitigate such damage could be crucial, including features like thicker encapsulants or improved backsheet materials to prevent structural weaknesses. For both panel types, the study supports the integration of inspection techniques, which is infrared thermography, into standard maintenance protocols to identify and address damage before it leads to significant performance degradation. At the practical level, these insights could influence site selection for solar farms, ensuring panels are deployed in areas where they can withstand lightning strikes effectively. Industry might also design installations with enhanced grounding systems or specialized mounting structures to further mitigate lightning impacts, ensuring long-term reliability.

CHAPTER 5

SUMMARY, CONTRIBUTIONS AND RECOMMENDATIONS FOR FUTURE WORKS

5.1 Summary of findings

In conclusion, this research employed a flow of method to assess lightning strike damages on monocrystalline and polycrystalline panels. Using Marx generator, high voltage impulse was generated on the samples with 30kV, 60kV and 90kV. Active thermography was carried out to detect the damages on the samples. Then, this research proposed a neural network architecture to classify the image datasets from the active thermography for damaged and undamaged samples.

The first objective was to analyse the lightning strike damage on the monocrystalline and polycrystalline panels. Based on the high voltage impulse on the solar panels, it was found that monocrystalline panels show less damages compared to polycrystalline panels. As the impulse voltage increases, the damage on the panel become more intense. Monocrystalline panels show minor defects on 60kV impulse and no damages on 30kV impulse. However, bubbles and dents were observed on the polycrystalline panels for 30kV and 60kV, respectively. Panels tested for 90kV does not show any damages.

The second objective was achieved using active thermography to detect the damages on the panels. Active thermography using tCam-Mini with FLIR Lepton 3.5 shows good results in detecting smaller defects and detecting the temperature difference as low as 0.1°C. Using active thermography, the damages can be observed on the thermal images with temperature variations on the damaged and undamaged parts of the samples. The damages on polycrystalline panels can be seen clearly on the thermal images. This rise and drop in temperature indicate damage on the panels because the affected region had significant variation which ranges from 0.5°C to 1.0°C.

The third objective was achieved by developing a CNN model for image classification of damaged and undamaged samples. The proposed neural network architecture shows 85.31% accuracy for the thermal images, 90.21% on grayscale images and 79% on contrast enhanced images. This result demonstrates that this architecture could effectively classify the damaged and undamaged samples for all types of images used in this research. With the comparison made with pre-trained models, it was found that the proposed architecture could classify all three types of images effectively. Pre-trained models perform well on only one or two types of image dataset from this research and F1 scores are lower than 80% for some image datasets. The error rates are also high where it shows more than 25% for certain instances with pre-trained models. The newly developed model demonstrated good performance in the classification, achieving high accuracy, precision and F1 score for all types of datasets.

5.2 Main contributions of the research

This study was able to give several contributions on the lightning damage assessment on solar panels using in-house portable infrared thermography camera with convolutional neural network (CNN) algorithm. The contributions are:

i. Polycrystalline panels show more damages on both panels with increasing intensity as the impulse voltage increases from 30kV to 60kV from bubbles to dents, compared to monocrystalline panels where it shows damages only on 60kV impulse voltage with minor peeling on the surface.

ii. Higher temperature with 60.6°C was observed on the panel with dent and 65.0°C and 64.6°C for the bubbles on the polycrystalline panels which is lower than the undamaged part.

iii. The proposed neural network architecture shows 85.31% accuracy for the thermal images, 90.21% on grayscale images and 79% on contrast enhanced images.

iv. Fewer studies were carried out on the lightning strike damage intensities on different types of crystalline panels with image classification technique using convolutional neural network. This study was able to identify the intensity of damage it causes on monocrystalline and polycrystalline panels with the integration of CNN algorithm to classify the image samples. The use of infrared thermography combined with CNN algorithms allows for the early detection of damage caused by lightning strikes.

5.3 Recommendation

For future research, several suggestions were recommended to improve the effectiveness and to open more prospects in this research area. The recommendations are:

i. For wider applicability, the usage of different kind of panels such as thin film, perovskite, organic solar panels, etc could be researched for lightning strike damage on structural level to assess their behaviour.

ii. Using a high-resolution thermal imaging camera would be beneficial to capture minor temperature variations indicative of lightning strike damages.

iii. CNN model with balanced architecture and computational efficiency to make the model work on various images could be researched to increase the diversity.

REFERENCES

[1] J. Shin, J. Park, and N. Park, “A method to recycle silicon wafer from end-of-life photovoltaic module and solar panels by using recycled silicon wafers,” *Solar Energy Materials and Solar Cells*, vol. 162, 2017, doi: 10.1016/j.solmat.2016.12.038.

[2] United Nations, “Goals 7: Ensure access to affordable, reliable, sustainable and modern energy for all,” United Nations. Accessed: Nov. 02, 2023. [Online]. Available: https://sdgs.un.org/goals/goal7

[3] United Nations, “Goals 13: Take urgent action to combat climate change and its impacts,” United Nations. Accessed: Nov. 02, 2023. [Online]. Available: https://sdgs.un.org/goals/goal13

[4] United Nations, “Goals 12: Ensure sustainable consumption and production patterns,” United Nations. Accessed: Nov. 02, 2023. [Online]. Available: https://sdgs.un.org/goals/goal12

[5] J. Dhilipan, N. Vijayalakshmi, D. B. Shanmugam, R. Jai Ganesh, S. Kodeeswaran, and S. Muralidharan, “Performance and efficiency of different types of solar cell material – A review,” *Mater Today Proc*, vol. 66, pp. 1295–1302, Jan. 2022, doi: 10.1016/j.matpr.2022.05.132.

[6] S. Sundaram, K. Shanks, and H. Upadhyaya, “Thin Film Photovoltaics,” in *A Comprehensive Guide to Solar Energy Systems*, Elsevier, 2018, pp. 361–370. doi: 10.1016/B978-0-12-811479-7.00018-X.

[7] M. A. Maehlum, “Energy informative the homeowner’s guide to solar panels, best thin film solar panels—Amorphous, cadmium telluride or CIGS,” *Last updated*, vol. 6, 2015.

[8] C. Lupangu and R. C. Bansal, “A review of technical issues on the development of solar photovoltaic systems,” *Renewable and Sustainable Energy Reviews*, vol. 73, pp. 950–965, 2017, doi: https://doi.org/10.1016/j.rser.2017.02.003.

[9] A. N. N. Afifah, Indrabayu, A. Suyuti, and Syafaruddin, “A review on image processing techniques for damage detection on photovoltaic panels,” *ICIC Express Letters*, vol. 15, no. 7, pp. 779–790, Jul. 2021, doi: 10.24507/icicel.15.07.779.

[10] A. Chokor, M. El Asmar, and S. V Lokanath, “A review of photovoltaic DC systems prognostics and health management: Challenges and Opportunities,” in *Annual Conference of the PHM Society*, 2016.

[11] U. Jahn, M. Herz, M. Köntges, D. Parlevliet, M. Paggi, and I. Tsanakas, *Review on infrared and electroluminescence imaging for PV field applications: International Energy Agency Photovoltaic Power Systems Programme: IEA PVPS Task 13, Subtask 3.3: report IEA-PVPS T13-12: 2018*. International Energy Agency, 2018.

[12] N. I. Ahmad *et al.*, "Lightning protection on photovoltaic systems: A review on current and recommended practices," Feb. 01, 2018, *Elsevier Ltd*. doi: 10.1016/j.rser.2017.07.008.

[13] N. H. Zaini *et al.*, "Lightning surge analysis on a large scale grid-connected solar photovoltaic system," *Energies (Basel)*, vol. 10, no. 12, Dec. 2017, doi: 10.3390/en10122149.

[14] R. Ebner, B. Kubicek, and G. Ujvari, "Non-destructive techniques for quality control of PV modules: Infrared thermography, electro- and photoluminescence imaging," in *IECON Proceedings (Industrial Electronics Conference)*, 2013, pp. 8104–8109. doi: 10.1109/IECON.2013.6700488.

[15] M. Papaelias *et al.*, "Inspection and Structural Health Monitoring techniques for Concentrated Solar Power plants," *Renew Energy*, vol. 85, pp. 1178–1191, Jan. 2016, doi: 10.1016/j.renene.2015.07.090.

[16] Á. H. Herraiz, A. P. Marugán, and F. P. G. Márquez, "A review on condition monitoring system for solar plants based on thermography," in *Non-Destructive Testing and Condition Monitoring Techniques for Renewable Energy Industrial Assets*, Elsevier, 2019, pp. 103–118. doi: 10.1016/B978-0-08-101094-5.00007-1.

[17] A. Haque, K. V. S. Bharath, M. A. Khan, I. Khan, and Z. A. Jaffery, "Fault diagnosis of Photovoltaic Modules," Jun. 01, 2019, *John Wiley and Sons Ltd*. doi: 10.1002/ese3.255.

[18] F. Lopez, C. Ibarra-Castanedo, V. De Paulo Nicolau, and X. Maldague, "Optimization of pulsed thermography inspection by partial least-squares regression," *NDT and E International*, vol. 66, pp. 128–138, 2014, doi: 10.1016/j.ndteint.2014.06.003.

[19] J. Isenberg and W. Warta, "Spatially resolved evaluation of power losses in industrial solar cells by illuminated lock-in thermography," *Progress in Photovoltaics: Research and Applications*, vol. 12, no. 5, pp. 339–353, Aug. 2004, doi: 10.1002/pip.547.

[20] A. Sinha, O. S. Sastry, and R. Gupta, "Detection and characterisation of delamination in PV modules by active infrared thermography," *Nondestructive Testing and Evaluation*, vol. 31, no. 1, pp. 1–16, Jan. 2016, doi: 10.1080/10589759.2015.1034717.

[21] B. Du, Y. He, Y. He, J. Duan, and Y. Zhang, "Intelligent Classification of Silicon Photovoltaic Cell Defects Based on Eddy Current Thermography and Convolution Neural Network," *IEEE Trans Industr Inform*, vol. 16, no. 10, pp. 6242–6251, Oct. 2020, doi: 10.1109/TII.2019.2952261.

[22] W. Mühleisen *et al.*, "Scientific and economic comparison of outdoor characterisation methods for photovoltaic power plants," *Renew Energy*, vol. 134, pp. 321–329, Apr. 2019, doi: 10.1016/j.renene.2018.11.044.

[23] R. Yang *et al.*, "Electromagnetic Induction Heating and Image Fusion of Silicon Photovoltaic Cell Electrothermography and

Electroluminescence," *IEEE Trans Industr Inform*, vol. 16, no. 7, pp. 4413–4422, Jul. 2020, doi: 10.1109/TII.2019.2922680.

[24] Á. Huerta Herraiz, A. Pliego Marugán, and F. P. García Márquez, "Photovoltaic plant condition monitoring using thermal images analysis by convolutional neural network-based structure," *Renew Energy*, vol. 153, pp. 334–348, Jun. 2020, doi: 10.1016/j.renene.2020.01.148.

[25] J. Muñoz, E. Lorenzo, F. Martínez-Moreno, L. Marroyo, and M. García, "An investigation into hot-spots in two large grid-connected PV plants," *Progress in Photovoltaics: Research and Applications*, vol. 16, no. 8, pp. 693–701, Dec. 2008, doi: 10.1002/pip.844.

[26] F. J. Suárez-Domínguez, M. B. Prendes-Gero, Á. Martín-Rodríguez, and A. Higuera-Garrido, "IR thermography applies to the detection of solar panel," *Revista de la Construcción*, vol. 14, no. 3, pp. 9–14, 2015.

[27] G. Acciani, G. B. Simione, and S. Vergura, "Thermographic analysis of photovoltaic panels," *Renewable Energy and Power Quality Journal*, vol. 1, no. 8, pp. 1245–1247, Apr. 2010, doi: 10.24084/repqj08.634.

[28] V. S. B. Kurukuru, A. Haque, M. A. Khan, and A. K. Tripathy, "Fault classification for photovoltaic modules using thermography and machine learning techniques," in *2019 International Conference on Computer and Information Sciences (ICCIS)*, IEEE, 2019, pp. 1–6.

[29] N. H. A. Rahim, Z. A. Baharudin, and M. N. Othman, "Investigation of Wave Propagation to PV-Solar Panel Due to Induced Overvoltage Generated by Lightning Impulse Generator," in *Advanced Science and Technology Letters*, Science & Engineering Research Support soCiety, Dec. 2013, pp. 15–22. doi: 10.14257/astl.2013.38.04.

[30] N. I. Ahmad, Z. Ali, M. Z. A. A. Kadir, M. Osman, N. H. Zaini, and M. H. Roslan, "Impacts of lightning-induced overvoltage on a hybrid solar PV–battery energy storage system," *Applied Sciences (Switzerland)*, vol. 11, no. 8, Apr. 2021, doi: 10.3390/app11083633.

[31] R. F. S. Wai, C.-W. Tsang, G.-K. Chu, T.-C. Pang, W.-F. Wong, and W.-C. Wong, "Prediction of future materials, maintenance and waste recovery costs on photovoltaics solar panels," 2018.

[32] M. D. Dafny Lydia, K. Sri Sindhu, and K. Gugan, "Analysis on solar panel crack detection using optimization techniques," *Journal of Nano- and Electronic Physics*, vol. 9, no. 2, 2017, doi: 10.21272/jnep.9(2).02004.

[33] M. Kaur and H. Singh, "A review: Comparison of silicon solar cells and thin film solar cells," *Int. J. Core Eng. Manag.(IJCEM)*, vol. 3, no. 2, pp. 15–23, 2016.

[34] U. K. Phoolwani, T. Sharma, A. Singh, and S. K. Gawre, "IoT Based Solar Panel Analysis using Thermal Imaging," in *2020 IEEE International Students' Conference on Electrical, Electronics and Computer Science, SCEECS 2020*, Institute of Electrical and Electronics Engineers Inc., Feb. 2020. doi: 10.1109/SCEECS48394.2020.114.

[35] W. D. Cyrs, H. J. Avens, Z. A. Capshaw, R. A. Kingsbury, J. Sahmel, and B. E. Tvermoes, “Landfill waste and recycling: Use of a screening-level risk assessment tool for end-of-life cadmium telluride (CdTe) thin-film photovoltaic (PV) panels,” *Energy Policy*, vol. 68, pp. 524–533, 2014, doi: 10.1016/j.enpol.2014.01.025.

[36] K. P. Bhandari and R. J. Ellingson, “An Overview of Hybrid Organic–Inorganic Metal Halide Perovskite Solar Cells,” in *A Comprehensive Guide to Solar Energy Systems: With Special Focus on Photovoltaic Systems*, Elsevier, 2018, pp. 233–254. doi: 10.1016/B978-0-12-811479-7.00011-7.

[37] V. Muteri *et al.*, “Review on life cycle assessment of solar photovoltaic panels,” Jan. 03, 2020, *MDPI AG*. doi: 10.3390/en13010252.

[38] M. A. Green *et al.*, “Solar cell efficiency tables (Version 53),” *Progress in Photovoltaics: Research and Applications*, vol. 27, no. 1, pp. 3–12, Jan. 2019, doi: 10.1002/pip.3102.

[39] M. Debbarma, K. Sudhakar, and P. Baredar, “Comparison of BIPV and BIPVT: A review,” *Resource-Efficient Technologies*, vol. 3, no. 3, pp. 263–271, Sep. 2017, doi: 10.1016/J.REFFIT.2016.11.013.

[40] M. Romero and J. González-Aguilar, “Solar thermal CSP technology,” Jan. 2014. doi: 10.1002/wene.79.

[41] R. Zakharchenko *et al.*, “Photovoltaic solar panel for a hybrid PV/thermal system,” in *Solar Energy Materials and Solar Cells*, May 2004, pp. 253–261. doi: 10.1016/j.solmat.2004.01.022.

[42] V. Gupta, M. Sharma, R. Pachauri, and K. N. D. Babu, “Impact of hailstorm on the performance of PV module: a review,” 2019, *Taylor and Francis Inc.* doi: 10.1080/15567036.2019.1648597.

[43] Y. Lozanov, S. Tzvetkova, and A. Petleshkov, “Faults in photovoltaic modules and possibilities for their detection by thermographic studies,” in *2019 11th Electrical Engineering Faculty Conference, BulEF 2019*, Institute of Electrical and Electronics Engineers Inc., Sep. 2019. doi: 10.1109/BulEF48056.2019.9030795.

[44] A. V. Shah *et al.*, “Thin-film silicon solar cell technology,” *Progress in Photovoltaics: Research and Applications*, vol. 12, no. 2–3, pp. 113–142, Mar. 2004, doi: 10.1002/PIP.533.

[45] J. Zhu, D. Wu, D. Montiel-Chicharro, T. R. Betts, and R. Gottschalg, “Realistic Adhesion Test for Photovoltaic Modules Qualification,” *IEEE J Photovolt*, vol. 8, no. 1, pp. 218–223, 2018, doi: 10.1109/JPHOTOV.2017.2775149.

[46] G. Oreski and G. Wallner, “Damp heat induced physical aging of PV encapsulation materials,” in *2010 12th IEEE Intersociety Conference on Thermal and Thermomechanical Phenomena in Electronic Systems, ITherm 2010*, Dec. 2010, pp. 1–6. doi: 10.1109/ITHERM.2010.5501297.

[47] G. Kleiss, J. Kirchner, and K. Reichart, “Quality and Reliability-sometimes the customer wants more … Summary and Conclusion,” 2015.

[48] A. L. Rosenthal and C. G. Lane, “Field test results for the 6 MW Carrizo solar photovoltaic power plant,” *Solar Cells*, vol. 30, no. 1–4, pp. 563–571, May 1991, doi: 10.1016/0379-6787(91)90088-7.

[49] U. Weber *et al.*, “Acetic acid production, migration and corrosion effects in ethylene-vinyl-acetate-(EVA-) based PV modules,” in *27th European Photovoltaic Solar Energy Conference and Exhibition*, 2012, pp. 2992–2995.

[50] S. Meyer *et al.*, “Snail Trails: Root Cause Analysis and Test Procedures,” *Energy Procedia*, vol. 38, pp. 498–505, 2013, doi: https://doi.org/10.1016/j.egypro.2013.07.309.

[51] A. Gosavi, P. Muley, J. Nirmal, S. Kulkarni, and R. Daryapurkar, “Solar Panel Fault Detection,” 2019. [Online]. Available: www.ijraset.com

[52] R. J. Mustafa, M. R. Gomaa, M. Al-Dhaifallah, and H. Rezk, “Environmental Impacts on the Performance of Solar Photovoltaic Systems,” *Sustainability*, vol. 12, no. 2, 2020, doi: 10.3390/su12020608.

[53] G. Di Lorenzo, R. Araneo, M. Mitolo, A. Niccolai, and F. Grimaccia, “Review of O&M Practices in PV Plants: Failures, Solutions, Remote Control, and Monitoring Tools,” *IEEE J Photovolt*, vol. 10, no. 4, pp. 914–926, Jul. 2020, doi: 10.1109/JPHOTOV.2020.2994531.

[54] Q. Wang, K. Paynabar, and M. Pacella, “Online automatic anomaly detection for photovoltaic systems using thermography imaging and low rank matrix decomposition,” *Journal of Quality Technology*, 2021, doi: 10.1080/00224065.2021.1948372.

[55] H. S. Rauschenbach and E. E. Maiden, “Breakdown phenomena in reverse biased silicon solar cells.,” 1972. [Online]. Available: https://api.semanticscholar.org/CorpusID:107880810

[56] S. Gallardo-Saavedra *et al.*, “Nondestructive characterization of solar PV cells defects by means of electroluminescence, infrared thermography, I–V curves and visual tests: Experimental study and comparison,” *Energy*, vol. 205, Aug. 2020, doi: 10.1016/j.energy.2020.117930.

[57] Y. Zhao, B. Lehman, J.-F. Palma, J. Mosesian, and R. Lyons, “Fault analysis in solar PV arrays under: Low irradiance conditions and reverse connections,” *Conference Record of the IEEE Photovoltaic Specialists Conference*, pp. 2000–2005, Dec. 2011, doi: 10.1109/PVSC.2011.6186346.

[58] Y. Zhao, J.-F. de Palma, J. Mosesian, R. Lyons, and B. Lehman, “Line–Line Fault Analysis and Protection Challenges in Solar Photovoltaic Arrays,” *IEEE Transactions on Industrial Electronics*, vol. 60, no. 9, pp. 3784–3795, 2013, doi: 10.1109/TIE.2012.2205355.

[59] M. Alam, F. Khan, J. Johnson, and J. Flicker, "PV faults: Overview, modeling, prevention and detection techniques," in *2013 IEEE 14th Workshop on Control and Modeling for Power Electronics, COMPEL 2013*, Dec. 2013, pp. 1–7. doi: 10.1109/COMPEL.2013.6626400.

[60] S. Lu, B. T. Phung, and D. Zhang, "A comprehensive review on DC arc faults and their diagnosis methods in photovoltaic systems," *Renewable and Sustainable Energy Reviews*, vol. 89, pp. 88–98, 2018, doi: https://doi.org/10.1016/j.rser.2018.03.010.

[61] C. Strobl and P. Meckler, "Arc Faults in Photovoltaic Systems," in *2010 Proceedings of the 56th IEEE Holm Conference on Electrical Contacts*, 2010, pp. 1–7. doi: 10.1109/HOLM.2010.5619538.

[62] J. Kalejs, "Junction box wiring and connector durability issues in photovoltaic modules," in *Reliability of Photovoltaic Cells, Modules, Components, and Systems VII*, N. G. Dhere, Ed., SPIE, 2014, p. 91790S. doi: 10.1117/12.2063488.

[63] M. R. Maghami, H. Hizam, C. Gomes, M. A. Radzi, M. I. Rezadad, and S. Hajighorbani, "Power loss due to soiling on solar panel: A review," *Renewable and Sustainable Energy Reviews*, vol. 59, pp. 1307–1316, 2016, doi: https://doi.org/10.1016/j.rser.2016.01.044.

[64] Z. A. Jaffery, A. K. Dubey, Irshad, and A. Haque, "Scheme for predictive fault diagnosis in photo-voltaic modules using thermal imaging," *Infrared Phys Technol*, vol. 83, pp. 182–187, Jun. 2017, doi: 10.1016/j.infrared.2017.04.015.

[65] W. Muehleisen *et al.*, "Outdoor detection and visualization of hailstorm damages of photovoltaic plants," *Renew Energy*, vol. 118, pp. 138–145, Apr. 2018, doi: 10.1016/j.renene.2017.11.010.

[66] E. L. Meyer and E. E. van Dyk, "Assessing the reliability and degradation of photovoltaic module performance parameters," *IEEE Trans Reliab*, vol. 53, no. 1, pp. 83–92, 2004, doi: 10.1109/TR.2004.824831.

[67] F. Bandou, A. H. Arab, and M. S. Belkaid, "Test Performance Electrical of the Photovoltaic Module in Two Different Environments," *Energy Procedia*, vol. 36, pp. 1018–1024, 2013, doi: https://doi.org/10.1016/j.egypro.2013.07.116.

[68] R. Meyta and F. V Savrasov, "To study the influence of snow cover on the power generated by photovoltaic modules," *IOP Conf Ser Mater Sci Eng*, vol. 81, Dec. 2015, doi: 10.1088/1757-899X/81/1/012110.

[69] B. Marion, R. Schaefer, H. Caine, and G. Sanchez, "Measured and modeled photovoltaic system energy losses from snow for Colorado and Wisconsin locations," *Solar Energy*, vol. 97, pp. 112–121, 2013, doi: https://doi.org/10.1016/j.solener.2013.07.029.

[70] J. Gwamuri, N. Heidari, T. Townsend, and J. Pearce, "Impact of Snow and Ground Interference on Photovoltaic Electric System Performance," *IEEE J Photovolt*, vol. PP, pp. 1–6, Dec. 2015, doi: 10.1109/JPHOTOV.2015.2466448.

[71] M. J. Adinoyi and S. A. M. Said, “Effect of dust accumulation on the power outputs of solar photovoltaic modules,” *Renew Energy*, vol. 60, no. C, pp. 633–636, 2013, [Online]. Available: https://EconPapers.repec.org/RePEc:eee:renene:v:60:y:2013:i:c:p:633-636

[72] H. Jiang, L. Lu, and K. Sun, “Experimental investigation of the impact of airborne dust deposition on the performance of solar photovoltaic (PV) modules,” *Atmospheric Environment - ATMOS ENVIRON*, vol. 45, pp. 4299–4304, Dec. 2011, doi: 10.1016/j.atmosenv.2011.04.084.

[73] S. A. M. Said and H. M. Walwil, “Fundamental studies on dust fouling effects on PV module performance,” *Solar Energy*, vol. 107, pp. 328–337, Sep. 2014, doi: 10.1016/J.SOLENER.2014.05.048.

[74] M. Saidan, A. G. Albaali, E. Alasis, and J. K. Kaldellis, “Experimental study on the effect of dust deposition on solar photovoltaic panels in desert environment,” *Renew Energy*, vol. 92, pp. 499–505, Jul. 2016, doi: 10.1016/J.RENENE.2016.02.031.

[75] M. Santhakumari and N. Sagar, “A review of the environmental factors degrading the performance of silicon wafer-based photovoltaic modules: Failure detection methods and essential mitigation techniques,” *Renewable and Sustainable Energy Reviews*, vol. 110, pp. 83–100, Aug. 2019, doi: 10.1016/J.RSER.2019.04.024.

[76] B. Figgis, D. Martinez Plaza, and T. Mirza, “PV soiling rate variation over long periods,” *Doha. DOI*, vol. 10, 2014.

[77] H. A. Kazem, A. H. A. Al-Waeli, M. T. Chaichan, K. Sopian, A. Gholami, and W. E. Alnaser, “Dust and cleaning impact on the performance of photovoltaic: an outdoor experimental study,” *Energy Sources, Part A: Recovery, Utilization, and Environmental Effects*, vol. 45, no. 1, pp. 3107–3124, Apr. 2023, doi: 10.1080/15567036.2023.2191064.

[78] A. Bouraiou *et al.*, “Experimental investigation of observed defects in crystalline silicon PV modules under outdoor hot dry climatic conditions in Algeria,” *Solar Energy*, vol. 159, Dec. 2018, doi: 10.1016/j.solener.2017.11.018.

[79] A. Bouraiou *et al.*, “Analysis and evaluation of the impact of climatic conditions on the photovoltaic modules performance in the desert environment,” *Energy Convers Manag*, vol. 106, pp. 1345–1355, Dec. 2015, doi: 10.1016/j.enconman.2015.10.073.

[80] D. C. Jordan and S. R. Kurtz, “Photovoltaic degradation rates—an analytical review,” *Progress in photovoltaics: Research and Applications*, vol. 21, no. 1, pp. 12–29, 2013.

[81] D. C. Jordan, J. H. Wohlgemuth, and S. R. Kurtz, “Technology and climate trends in PV module degradation,” National Renewable Energy Lab.(NREL), Golden, CO (United States), 2012.

[82] R. Dubey *et al.*, “Comprehensive study of performance degradation of field-mounted photovoltaic modules in India,” *Energy Sci Eng*, vol. 5, no. 1, pp. 51–64, 2017.

[83] D. Atsu, I. Seres, M. Aghaei, and I. Farkas, “Analysis of long-term performance and reliability of PV modules under tropical climatic conditions in sub-Saharan,” *Renew Energy*, vol. 162, pp. 285–295, Dec. 2020, doi: 10.1016/j.renene.2020.08.021.

[84] A. Sisodia and R. K. Mathur, “Impact of bird dropping deposition on solar photovoltaic module performance: a systematic study in Western Rajasthan,” *Environmental Science and Pollution Research*, vol. 26, Dec. 2019, doi: 10.1007/s11356-019-06100-2.

[85] M. D. Islam, M. A. Islam, and M. R. Khan, “Design of I-V Scanner to Analyze the Effects of Partial Shading due to Soiling and Bird-dropping on PV Panels,” in *2021 5th International Conference on Electrical Engineering and Information Communication Technology (ICEEICT)*, 2021, pp. 1–6. doi: 10.1109/ICEEICT53905.2021.9667805.

[86] M. Belik, “PV panels under lightning conditions,” in *Proceedings of the 2014 15th International Scientific Conference on Electric Power Engineering, EPE 2014*, IEEE Computer Society, 2014, pp. 367–370. doi: 10.1109/EPE.2014.6839446.

[87] T. Jiang and S. Grzybowski, “Electrical degradation of Photovoltaic modules caused by lightning induced voltage,” in *EIC 2014 - Proceedings of the 32nd Electrical Insulation Conference*, IEEE Computer Society, 2014, pp. 107–110. doi: 10.1109/EIC.2014.6869357.

[88] T. Jiang and S. Grzybowski, “Impact of lightning impulse voltage on polycrystalline silicon photovoltaic modules,” in *2013 International Symposium on Lightning Protection, SIPDA 2013*, IEEE Computer Society, 2013, pp. 287–290. doi: 10.1109/SIPDA.2013.6729225.

[89] T. Jiang and S. Grzybowski, “Influence of lightning impulse voltages on power output characteristics of Photovoltaic modules,” in *ICHVE 2014 - 2014 International Conference on High Voltage Engineering and Application*, Institute of Electrical and Electronics Engineers Inc., 2014. doi: 10.1109/ICHVE.2014.7035488.

[90] S. Sekioka, “An experimental study of sparkover between a rod and a photovoltaic panel,” in *2012 31st International Conference on Lightning Protection, ICLP 2012*, 2012. doi: 10.1109/ICLP.2012.6344268.

[91] C. Dechthummarong, S. Thepa, D. Chenvidhya, C. Jivacate, K. Kirtikara, and J. Thongpron, “Lightning impulse test of field-aged PV modules and simulation partial discharge within MATLAB,” in *2012 9th International Conference on Electrical Engineering/Electronics, Computer, Telecommunications and Information Technology, ECTI-CON 2012*, 2012. doi: 10.1109/ECTICon.2012.6254145.

[92] M. D. Calin, E. Helerea, and L. E. Aciu, “PV System Testing under Lightning Conditions,” in *2021 International Aegean Conference on*

Electrical Machines and Power Electronics, ACEMP 2021 and 2021 International Conference on Optimization of Electrical and Electronic Equipment, OPTIM 2021, Institute of Electrical and Electronics Engineers Inc., Sep. 2021, pp. 54–59. doi: 10.1109/OPTIM-ACEMP50812.2021.9590029.

[93] C. Christodoulou, V. Kontargyri, K. Damianaki, A. Kyritsis, I. Gonos, and N. Papanikolaou, “Lightning performance study for photovoltaic systems,” in *19th International Symposium on High Voltage Engineering. Pilsen. Czech Republic*, 2015.

[94] N. H. Zaini *et al.*, “On the effect of lightning on a solar photovoltaic system,” in *2016 33rd International Conference on Lightning Protection (ICLP)*, IEEE, 2016, pp. 1–4.

[95] E. Suresh Kumar, B. Sarkar, and D. Kumar Behera, “Failure of Photovoltaic Modules under Lightning and Thunderstorms,” 2013.

[96] A. S. Chaudhary and D. K. Chaturvedi, “Observing hotspots and power loss in solar photovoltaic array under shading effects using thermal imaging camera,” *Int. J. Electrical Machines and Drives, Journals Publications*, vol. 3, no. 1, pp. 15–23, 2017.

[97] M. Waqar Akram *et al.*, “Improved outdoor thermography and processing of infrared images for defect detection in PV modules,” *Solar Energy*, vol. 190, pp. 549–560, Sep. 2019, doi: 10.1016/j.solener.2019.08.061.

[98] A. S. M. Shihavuddin *et al.*, “Image based surface damage detection of renewable energy installations using a unified deep learning approach,” *Energy Reports*, vol. 7, pp. 4566–4576, Nov. 2021, doi: 10.1016/j.egyr.2021.07.045.

[99] Á. H. Herraiz, A. P. Marugán, and F. P. G. Márquez, “Optimal productivity in solar power plants based on machine learning and engineering management,” in *International Conference on Management Science and Engineering Management*, Springer, 2018, pp. 983–994.

[100] A. Kirsten Vidal de Oliveira, M. Aghaei, and R. Rüther, “Aerial infrared thermography for low-cost and fast fault detection in utility-scale PV power plants,” *Solar Energy*, vol. 211, pp. 712–724, Nov. 2020, doi: 10.1016/j.solener.2020.09.066.

[101] F. P. García Márquez and I. Segovia Ramírez, “Condition monitoring system for solar power plants with radiometric and thermographic sensors embedded in unmanned aerial vehicles,” *Measurement (Lond)*, vol. 139, pp. 152–162, Jun. 2019, doi: 10.1016/j.measurement.2019.02.045.

[102] X. Gao, E. Munson, G. P. Abousleman, and J. Si, “Automatic solar panel recognition and defect detection using infrared imaging,” in *Automatic Target Recognition XXV*, SPIE, May 2015, p. 94760O. doi: 10.1117/12.2179792.

[103] A. W. Kandeal *et al.*, “Infrared thermography-based condition monitoring of solar photovoltaic systems: A mini review of recent advances,” *Solar*

Energy, vol. 223, pp. 33–43, Jul. 2021, doi: 10.1016/j.solener.2021.05.032.

[104] S. Gallardo-Saavedra, L. Hernández-Callejo, M. D. C. Alonso-García, J. Muñoz-Cruzado-alba, and J. Ballestín-Fuertes, "Infrared thermography for the detection and characterization of photovoltaic defects: Comparison between illumination and dark conditions," *Sensors (Switzerland)*, vol. 20, no. 16, pp. 1–16, Aug. 2020, doi: 10.3390/s20164395.

[105] W. L. Khor, Y. K. Chen, M. Roberts, and F. Ciampa, "Automated detection and classification of concealed objects using infrared thermography and convolutional neural networks," *Sci Rep*, vol. 14, no. 1, Dec. 2024, doi: 10.1038/s41598-024-56636-8.

[106] C. Dunderdale, W. Brettenny, C. Clohessy, and E. E. van Dyk, "Photovoltaic defect classification through thermal infrared imaging using a machine learning approach," *Progress in Photovoltaics: Research and Applications*, vol. 28, no. 3, pp. 177–188, 2020.

[107] M. W. Akram, G. Li, Y. Jin, X. Chen, C. Zhu, and A. Ahmad, "Automatic detection of photovoltaic module defects in infrared images with isolated and develop-model transfer deep learning," *Solar Energy*, vol. 198, pp. 175–186, Mar. 2020, doi: 10.1016/J.SOLENER.2020.01.055.

[108] S. Ding, Q. Yang, X. Li, W. Yan, and W. Ruan, "Transfer Learning based Photovoltaic Module Defect Diagnosis using Aerial Images," in *2018 International Conference on Power System Technology (POWERCON)*, 2018, pp. 4245–4250. doi: 10.1109/POWERCON.2018.8602188.

[109] G. Cipriani, A. D'Amico, S. Guarino, D. Manno, M. Traverso, and V. Di Dio, "Convolutional neural network for dust and hotspot classification in PV modules," *Energies (Basel)*, vol. 13, no. 23, Dec. 2020, doi: 10.3390/en13236357.

[110] C. Bu, T. Liu, T. Wang, H. Zhang, and S. Sfarra, "A CNN-Architecture-Based Photovoltaic Cell Fault Classification Method Using Thermographic Images," *Energies (Basel)*, vol. 16, no. 9, May 2023, doi: 10.3390/en16093749.

[111] L. Bommes, T. Pickel, C. Buerhop-Lutz, J. Hauch, C. Brabec, and I. M. Peters, "Computer vision tool for detection, mapping, and fault classification of photovoltaics modules in aerial IR videos," *Progress in Photovoltaics: Research and Applications*, vol. 29, no. 12, pp. 1236–1251, 2021.

[112] S. Boubaker, S. Kamel, N. Ghazouani, and A. Mellit, "Assessment of Machine and Deep Learning Approaches for Fault Diagnosis in Photovoltaic Systems Using Infrared Thermography," *Remote Sens (Basel)*, vol. 15, no. 6, Mar. 2023, doi: 10.3390/rs15061686.

[113] W. Ahmed, A. Hanif, K. D. Kallu, A. Z. Kouzani, M. U. Ali, and A. Zafar, "Photovoltaic panels classification using isolated and transfer learned

deep neural models using infrared thermographic images," *Sensors*, vol. 21, no. 16, Aug. 2021, doi: 10.3390/s21165668.

[114] C. Tan, F. Sun, T. Kong, W. Zhang, C. Yang, and C. Liu, "A Survey on Deep Transfer Learning," in *Artificial Neural Networks and Machine Learning – ICANN 2018*, V. Kůrková, Y. Manolopoulos, B. Hammer, L. Iliadis, and I. Maglogiannis, Eds., Cham: Springer International Publishing, 2018, pp. 270–279.

[115] N. Kellil, A. Aissat, and A. Mellit, "Fault diagnosis of photovoltaic modules using deep neural networks and infrared images under Algerian climatic conditions," *Energy*, vol. 263, p. 125902, Jan. 2023, doi: 10.1016/J.ENERGY.2022.125902.

[116] H. Zhang, X. Hong, S. Zhou, and Q. Wang, "Infrared image segmentation for photovoltaic panels based on Res-UNet," in *Chinese conference on pattern recognition and computer vision (PRCV)*, Springer, 2019, pp. 611–622.

[117] A. Greco, C. Pironti, A. Saggese, M. Vento, and V. Vigilante, "A deep learning based approach for detecting panels in photovoltaic plants," in *Proceedings of the 3rd International Conference on Applications of Intelligent Systems*, 2020, pp. 1–7.

[118] R. H. Fonseca Alves, G. A. de Deus Júnior, E. G. Marra, and R. P. Lemos, "Automatic fault classification in photovoltaic modules using Convolutional Neural Networks," *Renew Energy*, vol. 179, pp. 502–516, Dec. 2021, doi: 10.1016/J.RENENE.2021.07.070.

[119] F. N. Iandola, S. Han, M. W. Moskewicz, K. Ashraf, W. J. Dally, and K. Keutzer, "SqueezeNet: AlexNet-level accuracy with 50x fewer parameters and< 0.5 MB model size," *arXiv preprint arXiv:1602.07360*, 2016.

[120] C. Szegedy *et al.*, "Going deeper with convolutions," in *Proceedings of the IEEE conference on computer vision and pattern recognition*, 2015, pp. 1–9.

[121] M. Tan and Q. Le, "Efficientnet: Rethinking model scaling for convolutional neural networks," in *International conference on machine learning*, PMLR, 2019, pp. 6105–6114.

APPENDICES

Appendix A1

Training progress of the developed CNN model

Thermal images

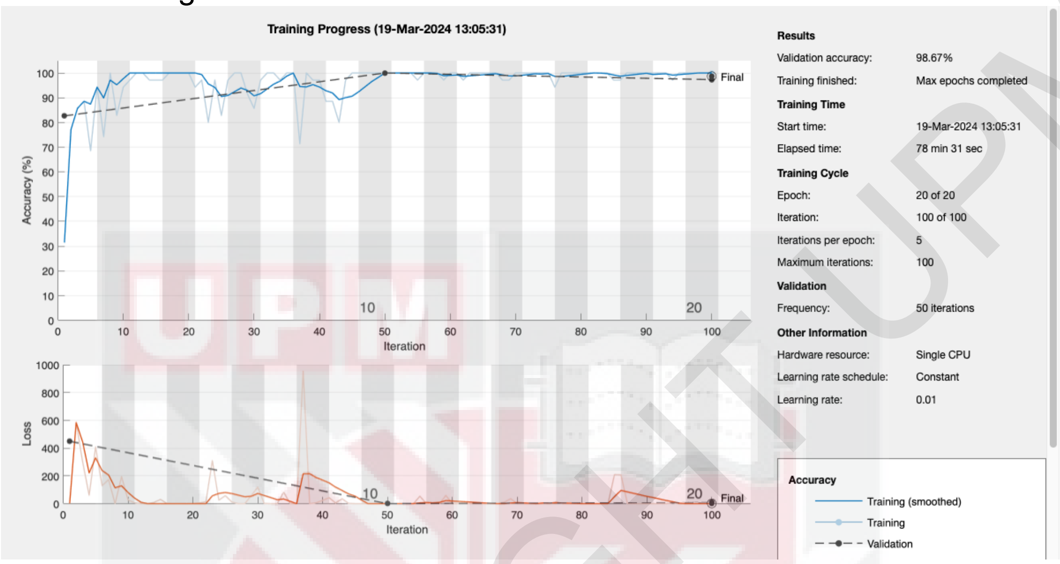

Grayscale images

Contrast enhanced images

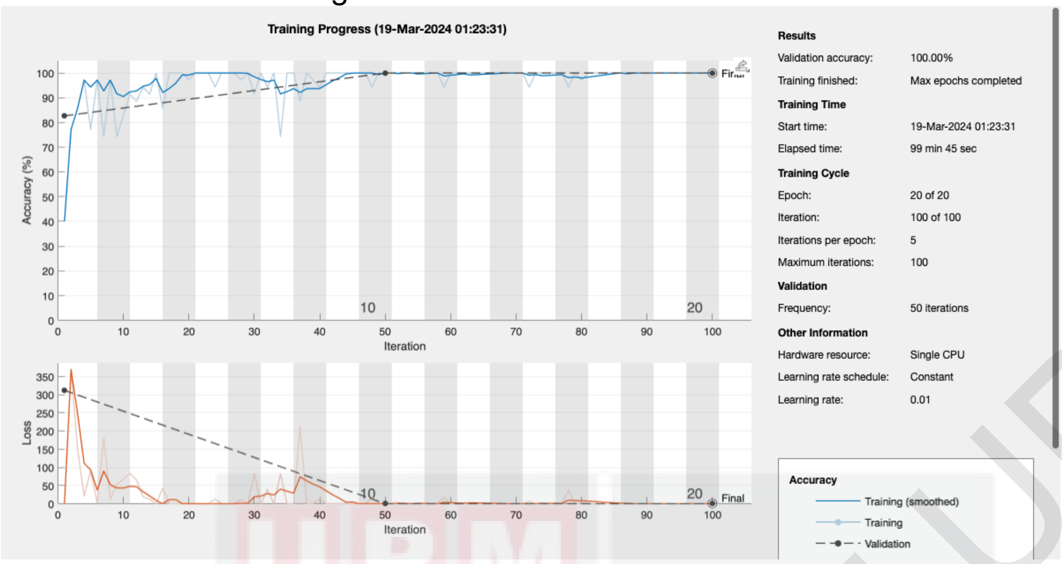

Appendix A2

Developed CNN model programme

Sample code for grayscale image training

```
%Load parameters for network initialization.
trainingSetup =
load("/Users/ormiilachandra/Desktop/params_2024_03_19__03_05_31bwtrained.mat");

%Import training and validation data.
imdsTrain = imageDatastore("/Users/ormiilachandra/Desktop/image data/b&w/bw-
train","IncludeSubfolders",true,"LabelSource","foldernames");
[imdsTrain, imdsValidation] = splitEachLabel(imdsTrain,0.7,"randomized");

% Resize the images to match the network input layer.
augimdsTrain = augmentedImageDatastore([227 227 1],imdsTrain);
augimdsValidation = augmentedImageDatastore([227 227 1],imdsValidation);

%Specify options to use when training.
opts = trainingOptions("sgdm",...
    "ExecutionEnvironment","auto",...
    "InitialLearnRate",0.01,...
    "MaxEpochs",20,...
    "MiniBatchSize",35,...
    "Shuffle","every-epoch",...
    "Plots","training-progress",...
    "ValidationData",augimdsValidation);

%Create the layer graph variable to contain the network layers.
lgraph = layerGraph();

%Add the branches of the network to the layer graph
tempLayers = [
    imageInputLayer([227 227 1],"Name","imageinput")
    convolution2dLayer([3 3],8,"Name","conv1","Padding","same","Stride",[3 3])
    batchNormalizationLayer("Name","batchnorm")
    reluLayer("Name","relu_14")
    convolution2dLayer([1 1],32,"Name","conv","Padding","same")
    reluLayer("Name","relu")
    maxPooling2dLayer([5 5],"Name","maxpool","Padding","same")
    convolution2dLayer([1 1],128,"Name","conv_1","Padding","same")
    batchNormalizationLayer("Name","batchnorm_1")
    reluLayer("Name","relu_15")
    convolution2dLayer([1 1],256,"Name","conv_2","Padding","same")
    reluLayer("Name","relu_1")];
lgraph = addLayers(lgraph,tempLayers);

tempLayers = [
    averagePooling2dLayer([5 5],"Name","avgpool2d","Padding","same")
    convolution2dLayer([2 2],8,"Name","conv_3","Padding","same")
    reluLayer("Name","relu_5")
    convolution2dLayer([1 1],256,"Name","conv_4","Padding","same")
    batchNormalizationLayer("Name","batchnorm_2")
    reluLayer("Name","relu_24")];
lgraph = addLayers(lgraph,tempLayers);
```

```
tempLayers = [
    depthConcatenationLayer(2,"Name","depthcat_1")
    convolution2dLayer([1 1],32,"Name","conv_5","Padding","same")
    batchNormalizationLayer("Name","batchnorm_3")
    reluLayer("Name","relu_9")
    maxPooling2dLayer([5 5],"Name","maxpool_1","Padding","same")
    convolution2dLayer([1 1],512,"Name","conv_6","Padding","same")];
lgraph = addLayers(lgraph,tempLayers);

tempLayers = [
    batchNormalizationLayer("Name","batchnorm_10")
    reluLayer("Name","relu_16")];
lgraph = addLayers(lgraph,tempLayers);

tempLayers = [
    reluLayer("Name","relu_25")
    convolution2dLayer([1 1],8,"Name","conv_22","Padding","same")
    reluLayer("Name","relu_12")];
lgraph = addLayers(lgraph,tempLayers);

tempLayers = [
    depthConcatenationLayer(2,"Name","depthcat_2")
    convolution2dLayer([1 1],128,"Name","conv_7","Padding","same")
    reluLayer("Name","relu_2")
    convolution2dLayer([1 1],512,"Name","conv_8","Padding","same")
    batchNormalizationLayer("Name","batchnorm_4")];
lgraph = addLayers(lgraph,tempLayers);

tempLayers = reluLayer("Name","relu_21");
lgraph = addLayers(lgraph,tempLayers);

tempLayers = [
    reluLayer("Name","relu_26")
    maxPooling2dLayer([5 5],"Name","maxpool_2","Padding","same")
    convolution2dLayer([1 1],32,"Name","conv_9","Padding","same")];
lgraph = addLayers(lgraph,tempLayers);

tempLayers = [
    reluLayer("Name","relu_17")
    convolution2dLayer([1 1],8,"Name","conv_11","Padding","same")
    batchNormalizationLayer("Name","batchnorm_11")
    reluLayer("Name","relu_18")
    convolution2dLayer([2 2],32,"Name","conv_23","Padding","same")
    reluLayer("Name","relu_19")];
lgraph = addLayers(lgraph,tempLayers);

tempLayers = reluLayer("Name","relu_20");
lgraph = addLayers(lgraph,tempLayers);

tempLayers = [
    concatenationLayer(2,2,"Name","concat")
    convolution2dLayer([1 1],256,"Name","conv_10","Padding","same")
    batchNormalizationLayer("Name","batchnorm_12")
    reluLayer("Name","relu_27")
    convolution2dLayer([1 1],512,"Name","conv_24","Padding","same","Stride",[1 2])
    reluLayer("Name","relu_13")];
lgraph = addLayers(lgraph,tempLayers);

tempLayers = [
    depthConcatenationLayer(2,"Name","depthcat1")
```

```
    groupedConvolution2dLayer([1 1],1,"channel-
wise","Name","groupedconv","Padding","same")
    batchNormalizationLayer("Name","batchnorm_5")
    reluLayer("Name","relu_8")
    maxPooling2dLayer([5 5],"Name","maxpool_3","Padding","same")
    convolution2dLayer([3 3],256,"Name","conv_12","Padding","same")
    reluLayer("Name","relu_22")];
lgraph = addLayers(lgraph,tempLayers);

tempLayers = [
    convolution2dLayer([3 3],32,"Name","conv_20","Padding","same")
    reluLayer("Name","relu_10")
    convolution2dLayer([1 1],256,"Name","conv_25","Padding","same")
    batchNormalizationLayer("Name","batchnorm_13")
    reluLayer("Name","relu_28")];
lgraph = addLayers(lgraph,tempLayers);

tempLayers = additionLayer(2,"Name","addition_2");
lgraph = addLayers(lgraph,tempLayers);

tempLayers = [
    averagePooling2dLayer([5 5],"Name","avgpool2d_1","Padding","same")
    convolution2dLayer([1 1],16,"Name","conv_13","Padding","same")
    batchNormalizationLayer("Name","batchnorm_9")
    convolution2dLayer([1 1],512,"Name","conv_14","Padding","same")
    reluLayer("Name","relu_7")];
lgraph = addLayers(lgraph,tempLayers);

tempLayers = [
    depthConcatenationLayer(2,"Name","depthcat_3")
    convolution2dLayer([1 1],256,"Name","conv_15","Padding","same")
    batchNormalizationLayer("Name","batchnorm_6")
    reluLayer("Name","relu_3")
    maxPooling2dLayer([5 5],"Name","maxpool_4","Padding","same")
    convolution2dLayer([1 1],64,"Name","conv_16","Padding","same","Stride",[2 2])
    reluLayer("Name","relu_4")
    convolution2dLayer([1 1],128,"Name","conv_17","Padding","same")];
lgraph = addLayers(lgraph,tempLayers);

tempLayers = [
    batchNormalizationLayer("Name","batchnorm_7")
    convolution2dLayer([1 1],256,"Name","conv_18","Padding","same")
    reluLayer("Name","relu_23")];
lgraph = addLayers(lgraph,tempLayers);

tempLayers = [
    convolution2dLayer([1 1],32,"Name","conv_21","Padding","same")
    reluLayer("Name","relu_11")];
lgraph = addLayers(lgraph,tempLayers);

tempLayers = [
    depthConcatenationLayer(3,"Name","depthcat_4")
    convolution2dLayer([1 1],1000,"Name","conv_19","Padding","same")
    batchNormalizationLayer("Name","batchnorm_8")
    reluLayer("Name","relu_6")
    dropoutLayer(0.3,"Name","dropout")
    fullyConnectedLayer(2,"Name","fc")
    softmaxLayer("Name","softmax")
    classificationLayer("Name","classoutput")];
lgraph = addLayers(lgraph,tempLayers);
```

```
% clean up helper variable
clear tempLayers;

%Connect all the branches of the network to create the network graph.
lgraph = connectLayers(lgraph,"relu_1","avgpool2d");
lgraph = connectLayers(lgraph,"relu_1","depthcat_1/in1");
lgraph = connectLayers(lgraph,"relu_24","depthcat_1/in2");
lgraph = connectLayers(lgraph,"conv_6","batchnorm_10");
lgraph = connectLayers(lgraph,"conv_6","relu_25");
lgraph = connectLayers(lgraph,"relu_16","depthcat_2/in2");
lgraph = connectLayers(lgraph,"relu_12","depthcat_2/in1");
lgraph = connectLayers(lgraph,"batchnorm_4","relu_21");
lgraph = connectLayers(lgraph,"batchnorm_4","relu_26");
lgraph = connectLayers(lgraph,"relu_21","depthcat1/in2");
lgraph = connectLayers(lgraph,"conv_9","relu_17");
lgraph = connectLayers(lgraph,"conv_9","relu_20");
lgraph = connectLayers(lgraph,"relu_19","concat/in1");
lgraph = connectLayers(lgraph,"relu_20","concat/in2");
lgraph = connectLayers(lgraph,"relu_13","depthcat1/in1");
lgraph = connectLayers(lgraph,"relu_22","conv_20");
lgraph = connectLayers(lgraph,"relu_22","addition_2/in1");
lgraph = connectLayers(lgraph,"relu_28","addition_2/in2");
lgraph = connectLayers(lgraph,"addition_2","avgpool2d_1");
lgraph = connectLayers(lgraph,"addition_2","depthcat_3/in1");
lgraph = connectLayers(lgraph,"relu_7","depthcat_3/in2");
lgraph = connectLayers(lgraph,"conv_17","batchnorm_7");
lgraph = connectLayers(lgraph,"conv_17","depthcat_4/in1");
lgraph = connectLayers(lgraph,"relu_23","conv_21");
lgraph = connectLayers(lgraph,"relu_23","depthcat_4/in3");
lgraph = connectLayers(lgraph,"relu_11","depthcat_4/in2");

%Train
[net, traininfo] = trainNetwork(augimdsTrain,lgraph,opts);
```

Sample code for grayscale image testing with trained network

```
location = 'image data/b&w/bw-test/damaged/*.jpeg';

ds = imageDatastore(location);
while hasdata(ds)
   img = read(ds);
   img2 = imresize(img,[227 227]);
   [YPred,probs] = classify(trainedNetwork_1,img2);
   label = YPred;
   title(string(label) + ", " + num2str(100*max(probs),3) + "%");
   disp(probs)
   figure, imshow(img2);
end
```

Appendix A3

Sample of output image classification from the CNN model

Thermal image (damaged)

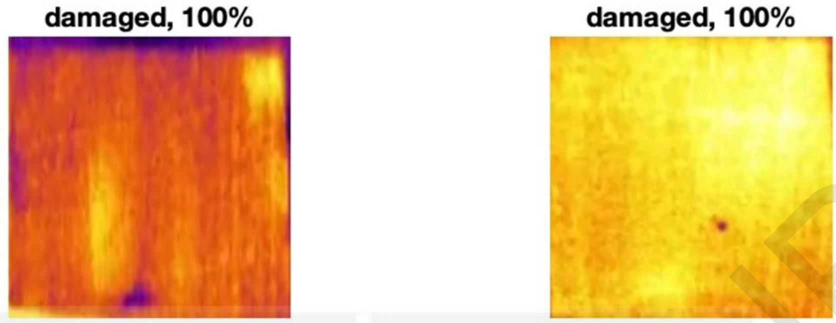

Thermal image (undamaged)

Grayscale (damaged)

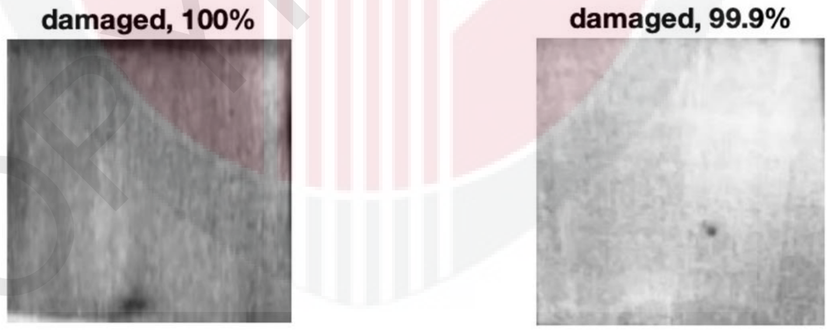

Grayscale (undamaged)

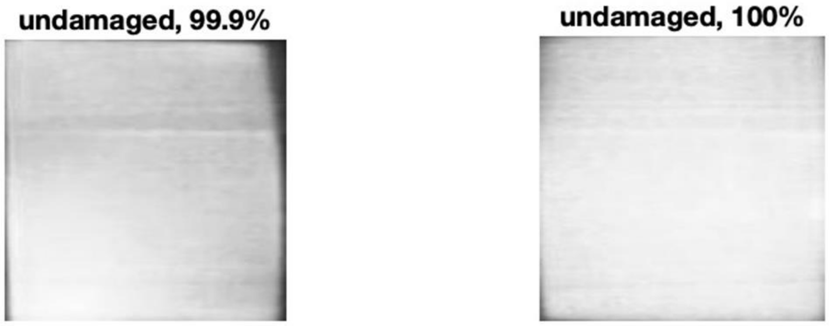

Contrast enhanced (damaged)

Contrast enhanced (undamaged)

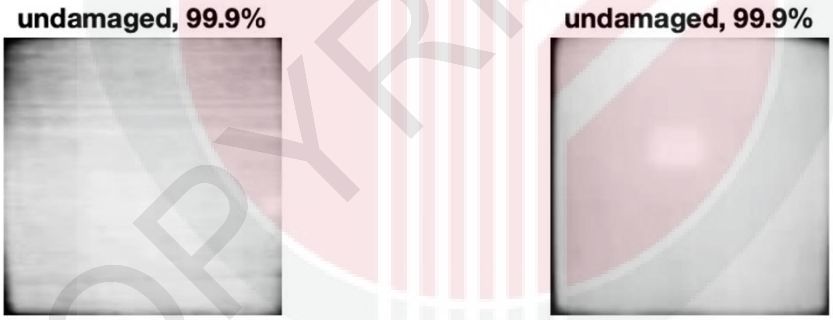

BIODATA OF STUDENT

Ormiila Chandrasegaran is a dedicated postgraduate student with a passion for exploring innovative solutions in the field of engineering. She completed her Bachelor's degree in Aerospace Engineering with honours from Universiti Putra Malaysia (UPM). During her undergraduate studies, her final year project comprised of integrating Internet of Things with active thermography and won gold under Structures and Materials category for Final Year Project Exhibition. She is also a recipient of Canada-ASEAN Scholarships and Educational Exchanges for Development (SEED) and was a visiting graduate research student at University of Regina, Canada from January 2023 to June 2023. Currently, Ormiila is pursuing Master of Science at Department of Aerospace Engineering, Faculty of Engineering, UPM researching on the damage detection and classification of lightning strike damage on solar panels under the supervision of Professor Ir Dr Faizal Mustapha.

LIST OF PUBLICATIONS

Chandrasegaran, O., Mustapha, F., Abdullah, M. N., Anwar, M., Mustapha, M., & Adzis, Z. (2024). Lightning damage assessment on solar panels using in-house portable infrared thermography camera with Convolutional Neural Network (CNN) algorithm. *Nondestructive Testing and Evaluation*, 1–43. https://doi.org/10.1080/10589759.2024.2410386